[doi.org/10.1016/j.isprsjprs.2022.01.017]

Land surface phenology retrievals for arid and semi-arid ecosystems

Qiaoyun Xie[1,*], Jamie Cleverly[1,2], Caitlin E Moore[3,4], Yanling Ding[1,5,*], Christopher C. Hall[1], Xuanlong Ma[6], Luke A. Brown[7], Cong Wang[8], Jason Beringer[3], Suzanne M. Prober[9], Craig Macfarlane[9], Wayne S. Meyer[10], Gaofei Yin[11], Alfredo Huete[1,*]

1. Faculty of Science, University of Technology Sydney, Sydney NSW 2007, Australia;
2. Terrestrial Ecosystem Research Network, College of Science and Engineering, James Cook University, Cairns, QLD 4811, Australia;
3. School of Agriculture and Environment, The University of Western Australia, Crawley, WA, 6010, Australia;
4. Institute for Sustainability, Energy and Environment, University of Illinois Urbana-Champaign, Urbana, IL, 61801, USA;
5. Key Laboratory of Geographical Processes and Ecological Security in Changbai Mountains, Ministry of Education, School of Geographical Sciences, Northeast Normal University, Changchun 130024, China;
6. College of Earth and Environmental Sciences, Lanzhou University, Lanzhou, Gansu 730000, China;
7. School of Geography and Environmental Science, University of Southampton, Highfield, Southampton, SO17 1BJ, United Kingdom;
8. Key Laboratory for Geographical Process Analysis & Simulation of Hubei Province/School of Urban and Environmental Sciences, Central China Normal University, Wuhan 430079, China;
9. Land and Water, Commonwealth Scientific and Industrial Research Organisation, Wembley, WA 6913, Australia;
10. School of Biological Sciences, The University of Adelaide, Adelaide, SA 5005, Australia;
11. Faculty of Geosciences and Environmental Engineering, Southwest Jiaotong University, Chengdu 610031, China

*Corresponding authors: Qiaoyun Xie (Qiaoyun.Xie@uts.edu.au); Yanling Ding (dingyl720@nenu.edu.cn); Alfredo Huete (Alfredo.Huete@uts.edu.au)

Abstract

Land surface phenology (LSP) plays a critical role in the regulation of photosynthesis, evapotranspiration, and energy fluxes. Significant progress has been made in extracting LSP information over large areas using satellite data, yet LSP retrievals remain a challenge over vast arid and semi-arid ecosystems because of sparse greenness, high variability and the lack of distinct annual patterns; for example, the MODerate Imaging Spectrometer (MODIS) Land Cover Dynamics Product MCD12Q2 that provides LSP metrics globally often failed to provide LSP information in these ecosystems. In this study, we used a modified threshold algorithm to extract LSP timing metrics, including the start, peak, and end of growing seasons, using the 16-day composite Enhanced Vegetation Index (EVI) time series from MODIS data. We applied this regionally customized algorithm across all arid and semi-arid climate regions of Australia (75% of the continental land area) encompassing shrublands, grasslands, savannas, woodlands, and croplands, extracting LSP metrics annually from 2003 to 2018, with up to two (phenology) seasons accounted for in each year. Our algorithm yielded an average of 64.9% successful rate of retrieval (proportion of pixels with retrieved LSP metrics) across 16 years in Arid and Semi-arid AUStralia (AS-AUS), which was a significant increase compared to the 14.5% rate of retrieval yielded in our study area by the global product and the major cause of the different performances between these two approaches was the different EVI amplitude restrictions utilized to avoid spurious peaks (i.e. EVI amplitude ≥ 0.1 used by the global

product and peak EVI ≥ time series average EVI used by our algorithm). Gross primary productivity (GPP) measurements at OzFlux eddy covariance (EC) tower sites were used to cross-compare with the presence/absence of growing seasons detected by our algorithm, and 97% of our retrieved seasons matched with those extracted using EC data. Preliminary tests at five OzFlux sites showed that our algorithm was robust to view angle-induced sensitivity of the input data and showed similar performance when using EVI data calculated using MODIS Nadir BRDF-Adjusted Reflectance product. Our retrieved LSP metrics revealed that vegetation growth in arid ecosystems is highly irregular and can occur at any time of the year, more than once in a year, or can skip a year. The proportion of pixels with two growing seasons was found to be correlated with the average annual precipitation of the study area ($p<0.01$), providing an estimation approach of LSP via rainfall. Our study improves the detection and measurement of vegetation phenology in arid and semi-arid regions by improving the spatial extend of LSP retrievals, which contributes to studies on LSP variations and dryland ecosystem resilience to climate change. More evaluation is planned for future work to assess and further improve the accuracy of the retrieved LSP metrics.

Key words:

Land surface phenology; Arid and semi-arid ecosystems; EVI; MODIS; Gross primary productivity; TERN OzFlux

1 Introduction

Vegetation phenology, the study of life cycle events in plants, including germination, bud break, flowering, and leaf senescence (Henebry and de Beurs, 2013), plays a critical role in the expression of photosynthesis and evapotranspiration, as well as land surface water, carbon and energy fluxes (Aires et al., 2008; White et al., 2009; Vivoni, 2012; Puma et al., 2013; Delbart et al., 2015; Ehleringer et al., 2019). Given this critical role, phenology has been widely studied to quantify the effect of climate change on terrestrial ecosystems. For example, increasingly early spring phenology has been associated with warming trends in the Northern Hemisphere (Myneni et al., 1997; Linderholm, 2006; Richardson et al., 2013; Xu et al., 2019). Additionally, the spatial and temporal dynamics of vegetation phenology can support the modelling of biospheric processes, detection of land cover and land use change, and agricultural management (Lymburner et al., 2011; Kennedy et al., 2014; Ma et al., 2015; Wang et al., 2017).

With nearly five decades of Earth observation developments, an increasing number of satellite sensors provide regular measurements of land surface properties with global coverage. Examples include the Advanced Very High Resolution Radiometer (AVHRR), the Moderate Resolution Imaging

Spectroradiometer (MODIS), and the Landsat and Copernicus Sentinel-2 missions. The increasing archive of satellite data has greatly benefited the observation of vegetation dynamics (Huete et al., 2002; Melaas et al., 2013; Keenan and Richardson, 2015). There have been a wide range of studies using various methods and satellite data, among which many have used vegetation index products to retrieve phenological metrics and most of those studies were focused on the Northern Hemisphere (Buitenwerf et al., 2015; Melaas et al., 2016; Wu et al., 2016; Liu et al., 2017; Peng et al., 2017; Thompson and Paull, 2017; Zhang et al., 2018a, 2018b; Moon et al., 2019; Bolton et al., 2020). The MODIS Land Cover Dynamics Product (MCD12Q2), referred to as the global product hereafter, provides global LSP from MODIS data (Zhang et al., 2003, 2006). Validations with field observations have demonstrated the reliability of this product over large regions, especially in temperate deciduous vegetation and agricultural areas. However, the algorithm used for the global product took a conservative approach that did not produce results if data were missing during transition periods or if the input vegetation index amplitude was very low (Ganguly et al., 2010; Gray et al., 2019), resulting in failed retrievals over arid and semi-arid areas (Broich et al., 2015).

Arid and semi-arid biomes cover around 40% of the Earth's terrestrial surface and provide important ecosystem services (James et al., 2013; Smith et al., 2019). Extensive arid regions occur in Australia, Africa, and extend from the Middle East through Central Asia. For example, Australia is covered with 75% arid and semi-arid (annual rainfall < 500 mm yr^{-1}) regions (Hughes, 2011). The positive anomaly in global land carbon uptake in 2010-11 was largely driven by semi-arid ecosystems in the Southern Hemisphere, with 60% of the global carbon uptake anomaly attributed to Australia's arid and semi-arid ecosystems (Poulter et al., 2014). The highly variable climate and irregular rainfall in arid and semi-arid regions can cause rapid vegetation greening and browning and hence irregular phenological patterns (Ma et al., 2013; Liu et al., 2017). These highly variable phenological patterns pose challenges for extracting LSP information from current remote sensing data products. Due to these issues, algorithms developed for LSP extraction from ecosystems with regular and defined phenological events often result in poorly-constrained or inaccurate retrievals from arid and semi-arid vegetation.

The lack of detailed characterization of biogeographical patterns in phenological cycles in arid and semi-arid regions greatly limits our understanding of ecosystem carbon exchange and future climate impacts on vegetation composition, functioning, and response to fire (Beringer et al., 2011, 2015; Moore et al., 2016; Z. Fu et al., 2019; Yu et al., 2020) and impedes our understanding of biodiversity as LSP is an indicator of biodiversity patterns (Vina et al., 2016). Studies have also reported that our knowledge of dryland ecosystems remains relatively limited because the structural and functional variability of vegetation dynamics occur at fine scales due to irregular rainfall patterns and due to underrepresentation of these ecosystems in long-term field measurements that are synthesized into larger networks (Smith et al., 2019).

It is a common practice to retrieve plant phenology from seasonal changes in satellite greenness indices using threshold-based algorithms that define phenology based on the date when a vegetation index reaches a predefined threshold (White et al., 1997), or curve-fitting algorithms that identify phenological metrics from a predefined mathematical function (Zhang et al., 2006; Zhang, 2015). The effectiveness of curve-fitting models, e.g. logistic methods, is dependent on the basic assumption that vegetation growth follows a well-defined S-shaped temporal profile, which would suffer from uncertainties in logistic curve fitting in arid and semi-arid areas due to the fact that the time series may deviate greatly from this sigmoid curve (Cao et al., 2015). As such, for Collection 6 of the global product (Friedl et al., 2019), the algorithm was changed from logistic methods used in Collection 5 to a threshold-based algorithm to increase the reliability of retrieved phenometrics in tropical, arid, and semi-arid ecosystems (Gray et al., 2019). Yet there are still missing values of the Collection 6 global product over large areas in arid and semi-arid ecosystems in Australia. Therefore, an algorithm designed for such areas is necessary to improve phenology monitoring in these globally significant ecosystems. For successful characterization of LSP in these regions, algorithms must be able to account for irregular phenological cycles that vary drastically in their timing, length, amplitude, and reoccurrence intervals (Ma et al., 2013; Cleverly et al., 2016a; Eamus et al., 2016).

Commonly used methods to validate satellite land surface phenology (LSP) include using traditional visual inspection (Liang and Schwartz, 2009); ground measurements of leaf area index; foliage biomass; leaf pigments (e.g. carotenoids and chlorophyll); time series of eddy covariance (EC) flux tower measurements (Nasahara and Nagai, 2015; Peng et al., 2017); multispectral images from time-lapse cameras located in carbon flux measurement sites (Peichl et al., 2015; Moore et al., 2016; Richardson et al., 2018a); photosynthetically active radiation; short-wave radiation sensor measurements; airborne hyperspectral/multi-spectral measurements; and citizen science observations (Zhang et al., 2018b). Satellite greenness indices have been directly related to EC tower carbon flux measurements across a wide range of ecosystems (Rahman et al., 2005; Gitelson et al., 2006; Ma et al., 2013). EC data represent fluxes which encompass diurnal and seasonal ecosystem processes, whilst satellite greenness measures operate at coarser time scales, but the two data sources are related and comparable.

Due to the importance of both arid and semi-arid regions as well as missing values of current LSP products in these regions, we aimed to improve the LSP retrieval algorithms that can subsequently be used to enhance our understanding of these variable ecosystem processes and functions. The objectives of this paper were (1) to improve LSP retrieval in terms of the rate of successful retrievals (proportion of pixels with successfully retrieved LSP metrics) in arid and semi-arid ecosystems, using Australia as a test case; (2) to evaluate the performance of our algorithm by comparing with the existing global LSP product MCD12Q2 and eddy covariance (EC) flux tower gross primary productivity data; and (3) to investigate the variability of LSP in these arid and semi-arid ecosystems and their response to climate drivers. We hypothesized that LSP would be characterized by intermittent growing seasons both intra-annually (i.e., with multiple growing seasons in a given year) and across years (i.e., with an absence of a detectable growing season in any given year), and that the seasonal amplitude of LSP would be smaller in arid and semi-arid regions of Australia than the threshold (amplitude ≥ 0.1) imposed by the latest version (Collection 6) of the global product.

2 Methods

2.1 Study area

For this study, we focused on arid and semi-arid regions in Australia according to the Köppen classification maps (Australian Bureau of Meteorology, 2016), which cover a wide geographical range (112 °E – 147 °E, 15 °S – 37 °S, Figure 1) (Davis et al., 2013) and shrubland, grassland, savanna, woodland, and cropland land cover types. The region is characterized by extremely low and unpredictable annual precipitation (100 – 500 mm y^{-1}, 30-year climatology 1981-2010) and high potential evaporation (2880 – 4000 mm y^{-1}, 30-year climatology 1961-1990) (www.bom.gov.au). The climate in Australia's arid and semi-arid regions can vary greatly from one year to the next, with much of the variability connected to the El Niño-Southern Oscillation (ENSO), a major air pressure and sea surface temperature relationship between the Australian/Indonesian region and the eastern Pacific (Heberger, 2012; Australian Bureau of Meteorology, 2014; Rogers and Beringer, 2017; Yang and Huang, 2021).

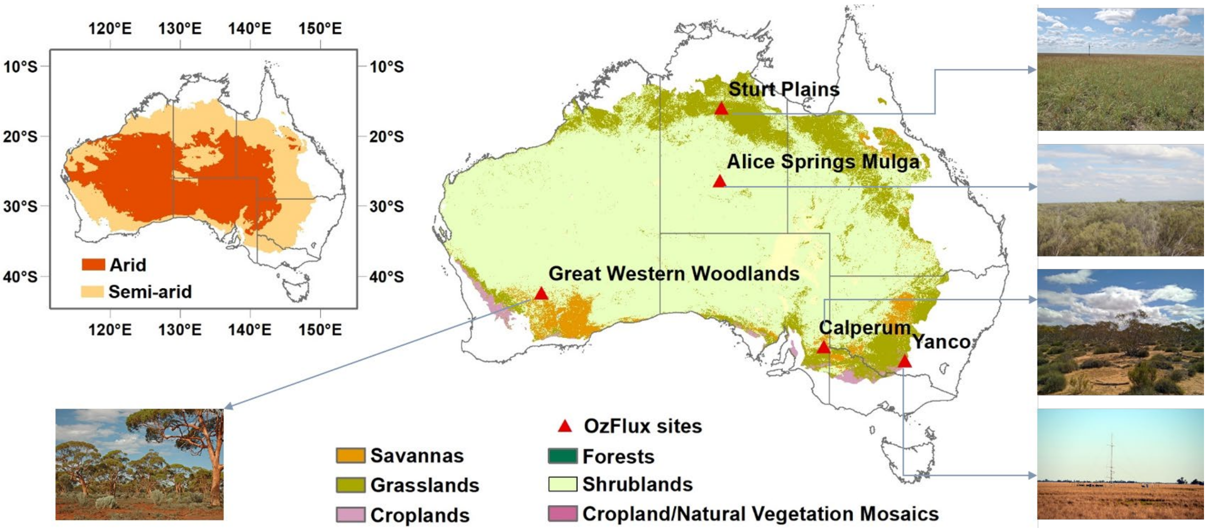

Figure 1. Study area. Upper left: extent of the arid and semi-arid regions in Australia according to the Köppen classification maps (http://www.bom.gov.au/). Right: land cover map showing vegetation types in the study area according to MODIS Land Cover Type (MCD12Q1) Version 6 data in 2018, and locations of five OzFlux eddy covariance sites in the study area. Forests include Evergreen Needleleaf Forests, Evergreen Broadleaf Forests, Deciduous Needleleaf Forests, Deciduous Broadleaf Forests, and Mixed Forests; Shrublands include Closed Shrublands and Open Shrublands; Savannas include Woody Savannas and Savannas. Figures of each site were obtained from http://www.ozflux.org.au/index.html

2.2 Data preprocessing

The data used for extraction of phenological metrics were from the 16-day 500 m MODIS vegetation index product MYD13A1, downloaded from NASA Land Processes Distributed Active Archive Centre (https://e4ftl01.cr.usgs.gov/). The MYD13A1 Enhanced Vegetation Index (EVI) (Huete et al., 2002) time series from July 2002 to June 2019 was used to calculate 500 m resolution gridded LSP metrics on an annual basis from 2003 to 2018. Note that for generating LSP metrics in each calendar year the length of the time series was extended by 6 months from the start and end of the calendar year (two years total). Similar to the global product, we used the EVI as input data because it provides a greater dynamic range than the normalized difference vegetation index (NDVI) (Zhang et al., 2003).

Quality control of the EVI images were achieved according to the quality assurance (QA) flags provided by the MYD13A1 product. We discarded observations with VI quality = '10' (Pixel produced, but most probably cloudy) or '11' (Pixel not produced due to other reasons than clouds), VI usefulness > 10 (Lowest quality; Quality so low that it is not useful; L1B data faulty; Not useful for any other reason/not processed), Aerosol Quantity = '11' (high), mixed clouds present, or adjacent cloud detected (Didan et al., 2015). We then gap-filled the low quality observations screened in the previous step per-pixel using cubic spline interpolation of the EVI time series (Dougherty et al., 1989). Finally, the EVI time series were filtered using the Savitsky-Golay smoothing method (Savitzky and Golay, 1964) a window size of 11 EVI composite periods and a 3rd order polynomial to further reduce remaining noise in the gap filled EVI time series.

2.3 *The AS-AUS phenology extraction algorithm*

Vegetation indices based on the contrast between the red region of the electromagnetic spectrum (where green vegetation strongly absorbs) and the near infrared region (where green vegetation strongly reflects) are commonly used to quantify vegetation greenness, e.g. the NDVI (Rouse Jr et al., 1974) and EVI (Huete et al., 2002). Time series of such vegetation indices are usually used to detect phenology metrics. In this study, we modified the threshold algorithm (Ma et al., 2015; Wang et al., 2018) to retrieve the LSP metrics, including the start, peak, end, and length of growing season(s) (SGS, PGS, EGS, LGS), in each year using two-year EVI time series data (Figure 2) and our approach is called Arid and Semi-arid AUStralia LSP, hereafter AS-AUS.

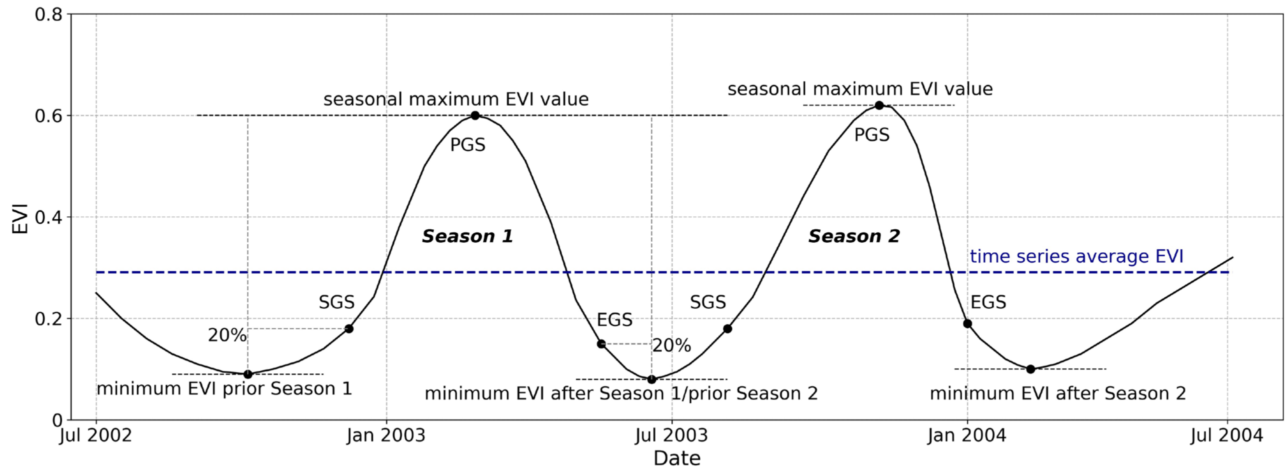

Figure 2. Conceptual diagram illustrating the algorithm for deriving phenological metrics in Arid and Semi-arid AUStralia (AS-AUS) from MODIS EVI time series showing example of two growing seasons in a year.

The conceptual definition of the AS-AUS LSP metrics is shown in Figure 2. Based on per-pixel EVI time series, we retrieved the phenological timing metrics for each season accounting for up to two seasons per year, similar to the global product. We defined the peak of growing season(s) (PGS) as the date when the EVI reached its maximum value during the growing season(s). Each peak is a local maximum value at least 128 days after the previous and before the subsequent peak to guarantee no more than three peaks in one year, and when three peaks occur in one calendar year, the two higher peaks were considered, similar to the global product algorithm (Gray et al., 2019). For defining the start of growing season(s) (SGS), like many other threshold algorithms (Wang et al., 2018), we chose a point during the green-up phase after EVI reached its minimum value prior to the growing season plus 20% of the green-up seasonal amplitude that equals the peak EVI value minus the minimum EVI value before PGS. Likewise, to define the end of growing season(s) (EGS), we used the point when the EVI reached its minimum value after the growing season plus 20% of the brown-down seasonal amplitude that equals the peak EVI value minus minimum EVI value after PGS. The length of growing season(s) (LGS) was the difference between EGS and SGS.

To avoid spurious peaks, amplitude restrictions are usually needed for threshold algorithms, e.g., the global product (Collection 6) requires that the seasonal amplitude between the minimum value and the peak value is greater than or equal to 0.1 (Gray et al., 2019). As such, LSP metrics would not be generated in the case of no growing seasons, or growing seasons with extremely low peak EVI values. As demonstrated using Alice Springs Mulga OzFlux site in Figure 3, EVI in most years does not meet the amplitude restriction of EVI ≥ 0.1 (thus would result in no LSP retrievals) except in 2017. However, GPP time series shows obvious growing seasons associated with rainfall in many years including 2011, 2014, 2015, and 2016. In this study, instead of using the same amplitude restriction for all pixels, we proposed to apply a pixel-wise seasonal amplitude restriction to capture more growing seasons with various amplitudes across arid and semi-arid Australia, i.e. for each pixel, we retrieved LSP metrics when the seasonal peak EVI value is greater than or equal to the time series average EVI value of this pixel (mean EVI value of the entire EVI time series from 2002 to 2019).

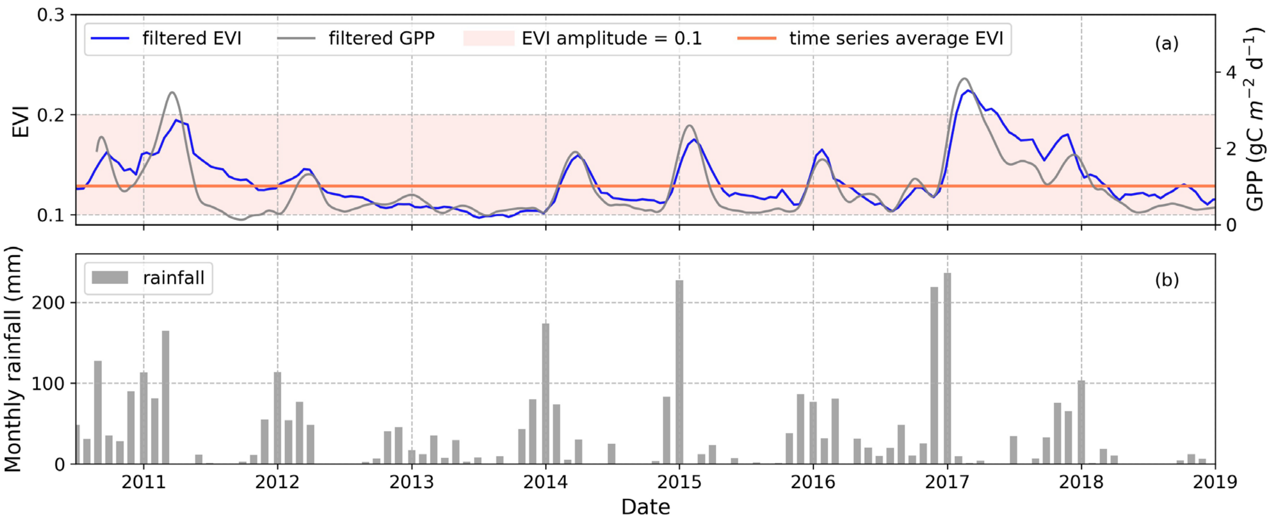

Figure 3. Illustration of two types of EVI amplitude threshold at Alice Springs Mulga flux tower site. (a) Filtered MODIS EVI and flux tower GPP time series, EVI amplitude equals 0.1 demonstrated by shaded areas, and time series average EVI; (b) Monthly rainfall from the 5 km gridded monthly rainfall data obtained from Bureau of Meteorology (www.bom.gov.au).

2.4 Characterisation and cross-comparison of LSP in arid and semi-arid Australia

To evaluate the threshold algorithm used to retrieve LSP in our study area, the rate of retrieval (RoR) was calculated using Eq. 1 for our algorithm and for the global product (Collection 6) each year from 2003 to 2018. As a case study, LSP metrics for the year when the global product was at its highest RoR were mapped for visual comparison between the global product and our LSP metrics. The absolute difference between SGS/PGS/EGS generated by AS-AUS and the global product MCD12Q2 was calculated for pixels with retrievals from both for inter-comparison.

$$RoR = \frac{number\ of\ pixels\ with\ retrieved\ LSP\ metrics}{number\ of\ total\ pixels\ in\ arid\ and\ semi{-}arid\ Australia} \times 100\% \qquad \text{Eq. 1}$$

Note that pixels with missing LSP values could be pixels with a growing season that algorithms failed to retrieve, or they could also be pixels without a growing season, in which case the missing values were not caused by the failure of LSP retrieval algorithms.

Flux towers provide continuous measurements of carbon, water and energy exchange between ecosystems and the atmosphere and often contribute to regional and global networks that make their data freely available, such as OzFlux (Beringer et al., 2016) and FLUXNET (Baldocchi et al., 2001). EC flux data were cross-compared with the satellite-derived AS-AUS LSP retrievals in this study. Five OzFlux sites located in the study area were selected to demonstrate and cross compare with LSP retrievals from satellite EVI time series, including two grassland sites (Sturt Plains and Yanco) that represent 16.1% of the land cover in our study area, a woodland/savanna site (Alice Springs Mulga) and a sparse evergreen woodland site (Calperum) that together represent 75.7% of the study area, and a woodland site (Great Western Woodlands) that represents 5.2% of the study area; note that these ecosystem descriptions slightly differ from the MODIS classifications for Australia (cf. Figure 1 and Table 1). Data from these sites provide valuable *in situ* information on the seasonal dynamics and inter-annual variations of ecosystem fluxes of carbon dioxide between the land surface and atmosphere, which we used to provide an independent measurement of vegetation growth to verify signals calculated from remote sensing approaches. NEE data from the five OzFlux sites were quality assured and quality checked (QA/QC) using the PyFluxPro tool developed by the OzFlux community (Isaac et al., 2017). PyFluxPro was also used to gap fill meteorological and gas flux variables, and partition NEE into ecosystem respiration (R_e) and GPP. For partitioning of NEE, we adopted the nocturnal temperature response approach in PyFluxPro using an artificial neural network to determine the R_e contribution to NEE, as detailed in Isaac et al. (2017) and Beringer et al. (2017), except for data from Alice Springs Mulga, which used Bilby TS to avoid inclusion of physically unrealistic values generated by standard methods (Cleverly et al., 2016b; Cleverly and Isaac, 2018; Tarin et al., 2020). Then, using Eq. 2, we calculated GPP.

$$GPP = R_e - NEE \qquad \text{Eq. 2}$$

With partitioned EC data, we extracted phenological metrics from the daily GPP time series data at each OzFlux site using the same threshold algorithm as for EVI data, and then compared them with those LSP metrics generated using EVI data. To keep the temporal resolution consistent with EVI data, daily GPP was averaged using a running window of 16 days from the current date through 15 days after the current date. First, seasons retrieved from the GPP time series were used to confirm whether those generated from satellite greenness data were real seasons rather than spurious ones. Then the agreement between LSP metrics generated from EVI and GPP data were evaluated using the coefficient of determination (R^2 value) and Root Mean Square Error (RMSE) as indicators of accuracy, although only three sites (Sturt Plains, Alice Springs Mulga, and Yanco) are suitable for direct comparison of SGS/PGS/EGS values where satellite greenness captures the seasonality of productivity (Restrepo-Coupe et al., 2016) and EVI synchronises with GPP. The Calperum (Mediterranean Mallee woodland) and Great Western Woodlands (Temperate Eucalypt woodland) sites are meteorological-driven and satellite greenness does not capture the seasonality of productivity at these two sites.

We illustrated the input and output of our algorithm at the five OzFlux sites that represent more than 95% of the land cover types in our study area (cf. Figure 1 and Table 1) to demonstrate the pixel-wise input and output data of our LSP extraction model. Note that within each land cover type, plant function types may differ greatly between different species, whereby these five sites may not be highly representative.

For climate analysis, 5 km gridded monthly rainfall and temperature data were obtained from Bureau of Meteorology (www.bom.gov.au) from 2003 to 2018, and then annual rainfall and annual mean temperature of the study area were calculated for each year and averaged across 16 years. P value was generated using Wald Test for the correlation between climate factors and the proportion of pixels with one, two, or no seasons.

Table 1. Names, coordinates, land cover type, annual mean temperature (AMT) and annual precipitation (AP) averaged from 2003 to 2018, for the OzFlux sites (http://www.ozflux.org.au/) shown in Figure 1. % of total land cover = area of certain land cover type * 100% / total area of arid and semi-arid Australia, calculated according to the IGBP land cover.

Site name	Lat (°S)	Lon (°E)	Land Cover Type	Site Description	% of land cover	AMT (°C)	AP (mm y^{-1})	GPP data	Site reference
Sturt Plains [AU-Stp]	-17.151	133.350	Grasslands	Grasslands	16.1%	27	730	2009-2019	(Beringer, 2013a)
Alice Springs Mulga [AU-ASM]	-22.275	133.225	Shrublands	Acacia woodland/ savanna	75.7%	23	390	2011-2019	(Cleverly, 2011)
Calperum [AU-Cpr]	-34.003	140.588	Shrublands	Mallee woodland	75.7%	18	270	2011-2019	(Tech, 2013)
Great Western Woodlands [AU-GWW]	-30.191	120.654	Savannas	Temperate Eucalypt woodland	4.0%	20	343	2013-2019	(MacFarlane, 2013)
Yanco [AU-Ync]	-34.989	146.291	Grasslands	Grasslands	16.1%	17	418	2013-2019	(Beringer, 2013b)

2.5 *Evaluation of the LSP retrieval algorithm*

To evaluate the sensitivity of our algorithm to input data and seasonal amplitude restrictions, and to investigate the cause of underperformance of the global product in arid and semi-arid ecosystems, we used the same input data and the same amplitude restriction (greater than or equal to 0.1) as the global product. We hypothesized that the seasonal amplitude of LSP would be smaller in arid and semi-arid regions of Australia than the threshold (EVI amplitude ≥ 0.1) imposed by the global product and we tested it at five OzFlux sites as mentioned above. The input data in this study for LSP extraction was the MYD13A1 EVI time series (Huete et al., 1999). In contrast, the global product used EVI calculated using the MODIS Nadir BRDF-Adjusted Reflectance (NBAR) product (MCD43A4) as input data to generate phenological metrics, in which NBAR data provides surface reflectances in which view angle effects have been removed. Both cloud and aerosol contamination is minimized for MYD13A1 and MCD43A4 (NBAR) data (Schaaf et al., 2002; Zhang et al., 2006). First, the EVI calculated using daily gridded 500 m MODIS NBAR product MCD43A4 was used as input data of our algorithm and the output metrics were compared with those using EVI from the 16-day gridded 500 m MODIS vegetation index product MYD13A1.

The amplitude restriction was the major difference between our algorithm and the global product algorithm, and other minor differences include input data and start/end segment search windows of SGS and EGS, i.e. 185 days to 30 days before/after the PGS used in the global product and 128 days to 16 days before/after the PGS used in our study. To investigate whether the differences in amplitude restriction is the major cause of underperformance of the global product in arid and semi-arid Australia, we applied this restriction in our threshold algorithm at the five selected OzFlux sites and compared the performance with our original algorithm and the global product.

3 Results

3.1 *LSP retrievals in arid and semi-aid Australia*

Throughout arid and semi-arid Australia (AS-AUS), the proportion of pixels with detected vegetation growth varied significantly from year to year across the 16 years, as shown in Figure 4, ranging from around 40% (in 2005) to nearly 90% (in 2011) (Figure 4b), among which most areas showed one growing season and a small percentage (under 10% of the study area) showed a second season. In contrast, the global product detected vegetation growth across a much smaller proportion of the area, ranging from around 10% (in 2013) to nearly 20% (in 2010) (Figure 4a). As shown in Figure 5, across AS-AUS, the RoR of the global product (MCD12Q2) was below 20% during the 16 years, whilst the

RoR of AS-AUS was much higher than that of the MCD12Q2, ranging from 40% to above 80%. The 16-year average RoR was 14.5% and 64.9% for MCD12Q2 and AS-AUS, respectively.

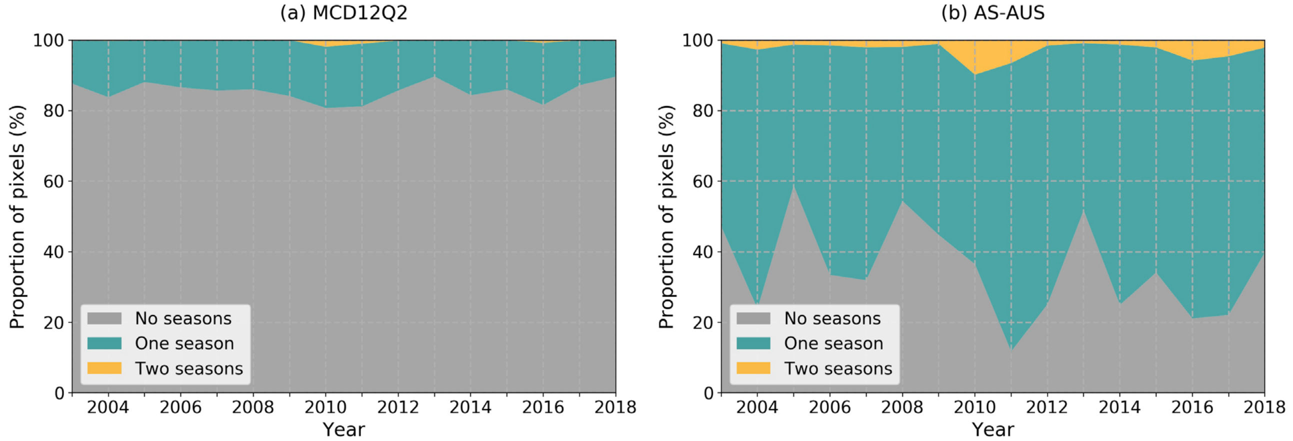

Figure 4. Proportion of pixels with no seasons, one season, and two seasons each year in arid and semi-arid Australia from 2003 to 2018 generated by (a) the global product MCD12Q2, and (b) our study in Arid and Semi-arid AUStralia (AS-AUS).

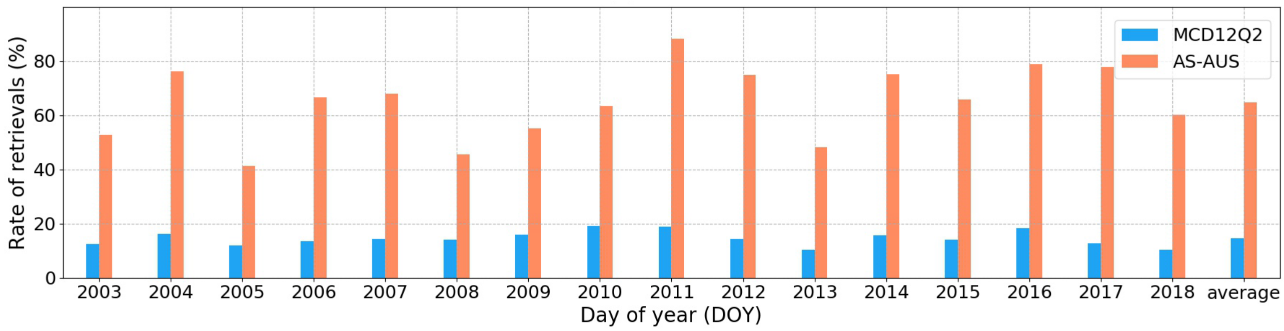

Figure 5. Rate of successful retrieval (% of total arid and semi-arid Australia retrieved) of MCD12Q2 and the Arid and Semi-arid - AUStralia (AS-AUS) metrics each year from 2003 to 2018.

Figure 6 demonstrates the start/peak/end of growing seasons (SGS/PGS/EGS) generated from the global product and our AS-AUS (Figure 6a-f) and histograms of the absolute difference between metrics retrieved by both AS-AUS and the global product (Figure 6g-i) for the first season in 2010, a year during the La Niña event when rainfall significantly increased. Through visual comparison, the metrics provided by the global product showed high consistency with the AS-AUS counterparts where both retrievals succeeded (Figure 6a-f), whilst AS-AUS performed better with successful retrievals in more areas. For pixels with retrievals from both datasets (1,048,575 pixels in total), around 90% of them showed a difference within 32 days (which equals two composite periods of the 16-day EVI) for SGS and PGS, and around 85% of them showed a difference within 32 days for EGS (Figure 6g-i), confirming the high consistency between AS-AUS and the global product.

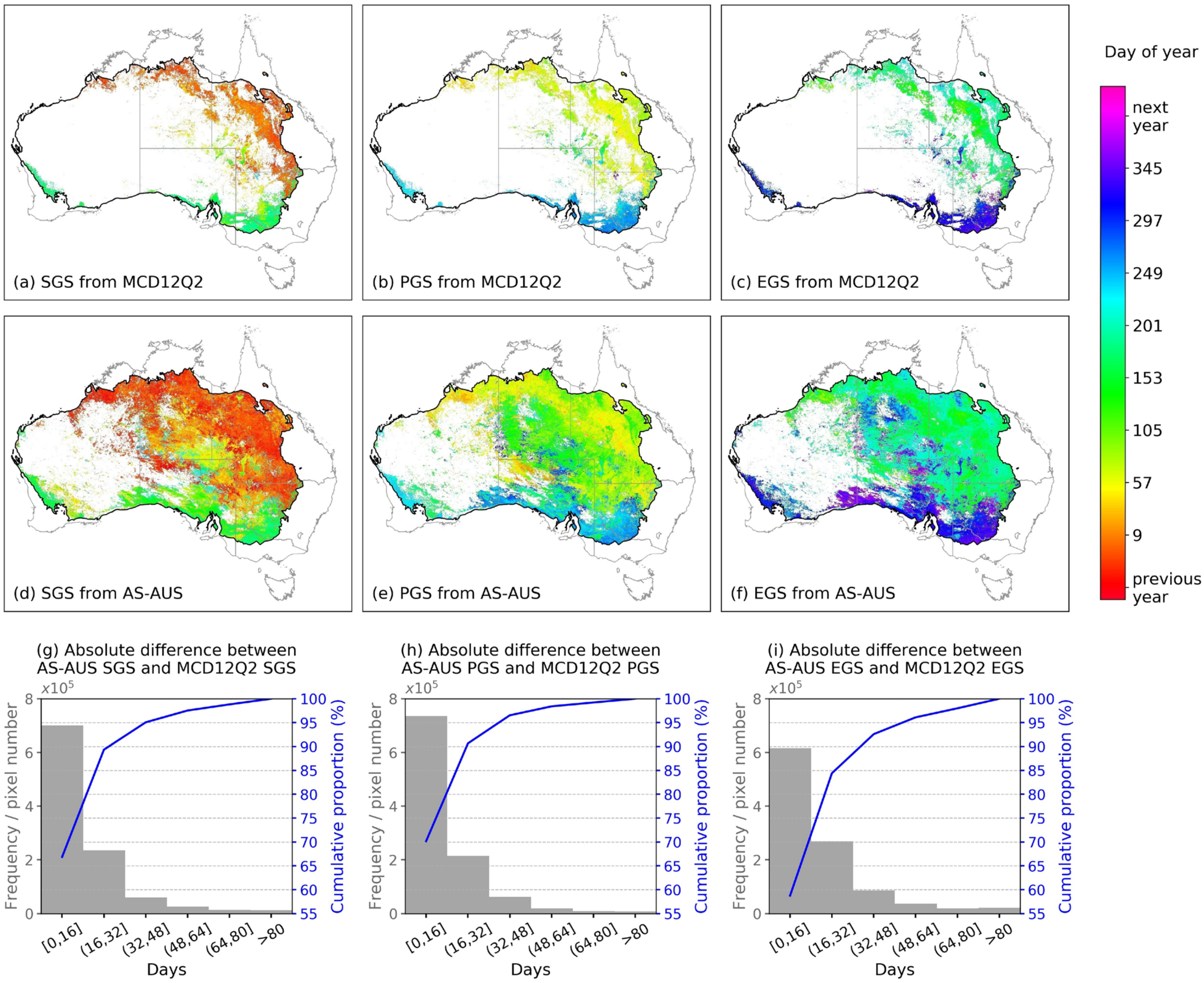

Figure 6. (a)-(f) Start (SGS)/peak (PGS)/end (EGS) of the first growing season in 2010 generated from the global product and the AS-AUS from this study and (g)-(i) the absolute difference between SGS/PGS/EGS generated by both AS-AUS and the global product MCD12Q2 (1,048,575 pixels in total). In (a)-(f), the black line highlights the boundary of arid and semi-arid areas, and white pixels within the arid and semi-arid boundary represent areas without detectable seasons.

Vegetation growing seasons in arid and semi-arid Australia showed extreme temporal and spatial variation, particularly in grasslands and shrublands (cf. Figure 1, Figure 6). In terms of temporal variation, vegetation growing seasons occurred throughout the entire year of 2010, starting from before the beginning of the year in many northern and eastern areas, extending across the end of the year in some southern areas, and occurring at any time of year across the study area. In terms of spatial variation, the patterns in our study area showed a general gradient from north to south, with growing seasons starting earlier in the north during the previous year, than those in the south, where SGS occurred during late summer or autumn (day of year around 50-150) (Figure 6d). Previous studies have reported that temperature limits the potential growing season of vegetation but, if there is no water available, plants will not grow (Winslow et al., 2003). In arid and semi-arid ecosystems, vegetation phenology is highly driven by rainfall events. Therefore, in years when rainfall is extremely low, vegetation will appear dormant, as evident from the vast areas in Western Australia where no LSP episodes were detected in 2010 (Figure 6).

3.2 Demonstration and evaluation of LSP episodes at selected OzFlux sites

Figure 7 shows examples of temporal variability of the vegetation greenness (EVI), GPP, and SGS and EGS from 2010 to 2018 for five selected OzFlux sites, which represent more than 95% of the land cover types in our study area (cf. Figure 1 and Table 1). The EVI time series of these sites showed distinct seasonality. Across the sites with varied climate conditions, higher peak EVI values were associated with higher annual rainfall amounts (cf. Table 1, Figure 7). Land surface phenology in arid and semi-arid Australia was highly variable and can also be non-annual (skipping a year, or having more than one season in a year), as shown in Figure 7. For example, at the Alice Springs Mulga woodland/savanna site, the phenological timing, length, and EVI amplitude varied drastically throughout 9 years with no LSP episode detected in 2013, whilst two LSP episodes were detected in 2010 and 2017. By contrast, at the Sturt Plains grassland site, all LSP metrics occurred every year with the peak of the growing season in late summer/early autumn (around February-March). 97% of seasons (31 out of 32 seasons) retrieved by our algorithm matched with those generated with GPP (Table 2), and one season in 2018 at Alice Springs Mulga generated using EVI did not match the GPP season due to low GPP amplitude. Our algorithm was designed to avoid recognising spurious local peak EVI values as the seasonal peak EVI. As such, LSP metrics were not produced when the peak EVI value was lower than the mean EVI value of the entire time series. An example of such a scenario is the peak EVI in 2016 at Calperum, which was below the restriction of our algorithm (greater than mean EVI value of the entire time series), thus it was not considered as a growing season and no LSP metrics were retrieved. However, this restriction could result in some missing values in areas of vegetation when the peak value of the current year is extremely low. For example, the LSP values in 2014 at the Calperum woodland site were missed due to the low seasonal peak value caused by a wildfire; part of the Calperum site was burned by a wildfire in January 2014 after more than 10 days with day time temperatures over 35°C (Sun et al., 2016).

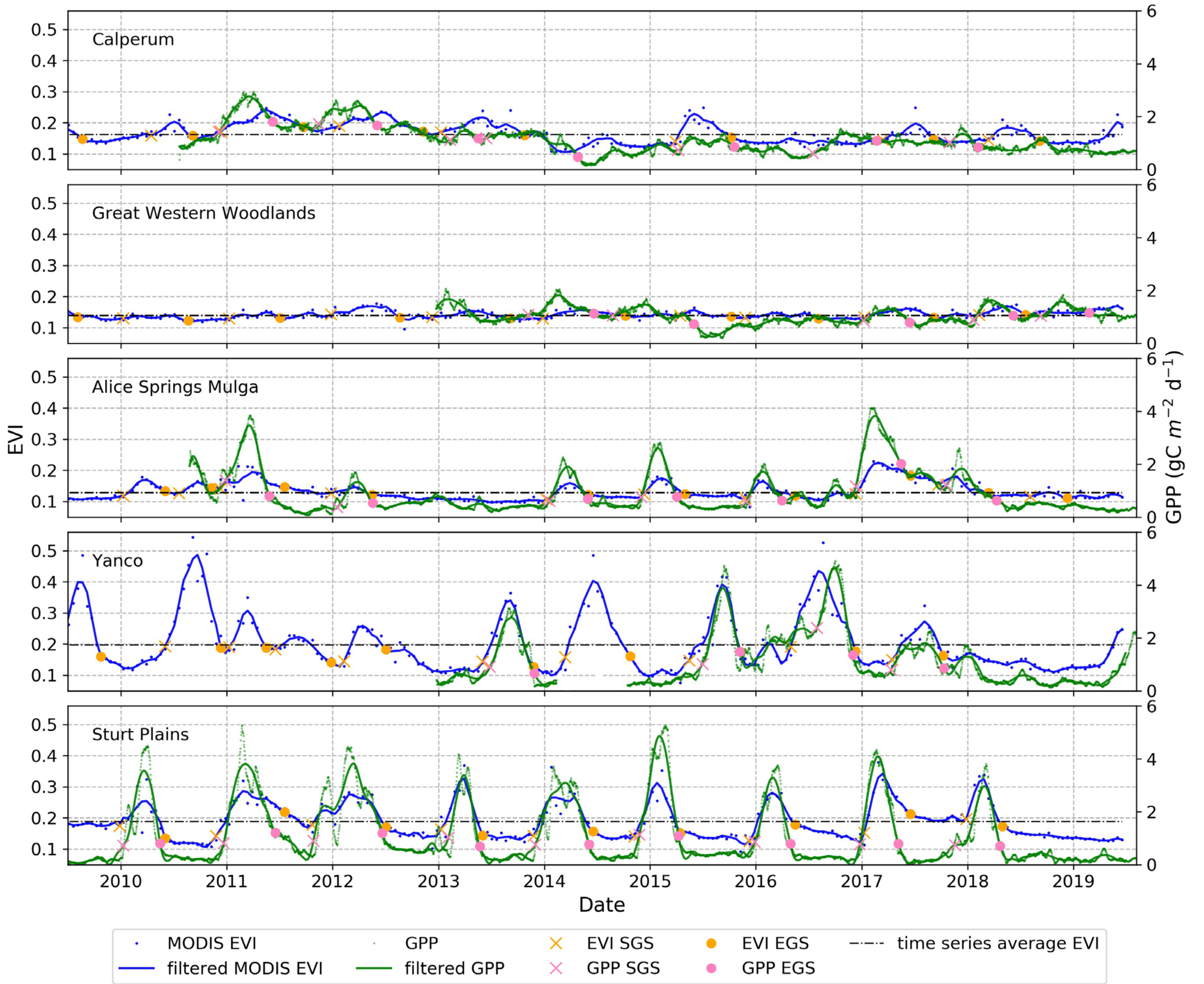

Figure 7. Temporal variability of the characterized LSP episodes from 2010 to 2018 for the five OzFlux sites: Calperum, Great Western Woodlands, Alice Springs Mulga, Stuart Plains, and Yanco. The MAP of each site increases from top to down in the figure according to Table 1. Green and navy dots represent 16-day running average GPP and 16-day EVI time series, respectively. Green and navy lines represent the GPP and EVI time series after SG filtering, respectively. Pink and orange signs represent the identified start and end of growing season points using GPP and EVI, respectively.

Table 2. Number of LSP episodes retrieved using EVI and GPP, respectively.

Site name	Years retrieved using both EVI and GPP	Growing seasons from EVI	Growing seasons from GPP
Sturt Plains [AU-Stp]	9	9	9
Alice Springs Mulga [AU-ASM]	8	8	7
Calperum [AU-Cpr]	8	6	7
Great Western Woodlands [AU-GWW]	5	5	5
Yanco [AU-Ync]	5	4	4

16-day EVI and 16-day running averaged daily EC tower GPP time series showed good convergences through visual comparison, at the grassland and savanna sites, i.e. Sturt Plains, Alice Springs Mulga, and Yanco (Figure 7). By contrast, EVI patterns did not match those of tower GPP at Calperum

(Mediterranean Mallee woodland) and Great Western Woodlands (Temperate Eucalypt woodland). Studies have reported that these ecosystems are meteorological-driven and changes in plant greenness do not synchronise with changes in photosynthesis, therefore, satellite greenness does not capture the seasonality of productivity (Restrepo-Coupe et al., 2016). Despite the fact that the EVI and GPP are not synchronised at these two sites, the GPP time series still provides key insights into whether a season seen from the EVI time series was a real growing season or a spurious one. As such, in years when both EVI and GPP data were available at these five sites, the LSP episodes from EVI data were all confirmed by the LSP episodes from GPP data, except the season in 2018 at Alice Springs Mulga, which had a very low amplitude of EVI and GPP (Figure 7, Table 2).

Figure 8 shows the cross-comparison between LSP metrics retrieved in our study from 2010 to 2018 and those retrieved using GPP data during the same period at all five OzFlux sites (red colour) and at the three grassland/savanna sites (blue colour) when excluding Calperum and Great Western Woodlands for reasons mentioned above. Therefore, only these three sites represent proper evaluation of LSP metrics retrieved from satellite EVI against those retrieved using flux tower GPP. The agreements between phenological metrics generated using EVI and GPP time series of all five sites were reasonably high with coefficients of determination (R^2) equalling 0.76, 0.68, and 0.52 and RMSE equalling 45.51, 48.95, and 62.09 days, for SGS, PGS, and EGS, respectively. The accuracy was much higher at the three grassland/savanna sites with R^2 equalling 0.91, 0.97, and 0.94 and RMSE equalling 28.49, 16.70, and 24.56 days, for SGS, PGS, and EGS, respectively. Note that the input data of our LSP retrieval algorithm were 16-day composite EVI, hence an RMSE value of 62.09 is within 4 compositing dates, and an RMSE value of 28.49 is within 2 compositing periods.

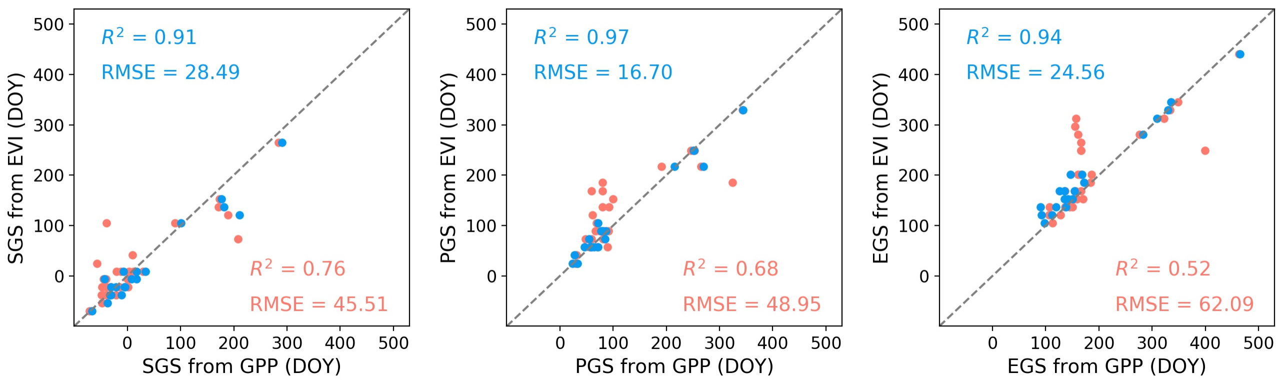

Figure 8. Cross-comparison between AS-AUS phenological metrics retrieved from EVI time series and those retrieved from GPP data at all five OzFlux sites (in red colour; n=29 for the five sites altogether) and at three grassland and savanna sites (in blue colour; n=20 for the three sites altogether), Sturt Plains, Alice Springs Mulga, and Yanco. Here day of year (DOY) lower than 0 means days before the beginning of the year, and DOY exceeding 365 are in the next year.

3.3 *Spatial and temporal variability of vegetation phenology in arid and semi-arid Australia*

The LSP metrics generated from our model show that vegetation seasons in arid and semi-arid areas of Australia are highly variable and can occur at any time of the year (albeit very unlikely in November due to low rainfall amounts in July through October), or more than once in a year, and could skip a year. For example, the histogram of per-pixel PGS in arid and semi-arid Australia varies greatly from year to year (Figure 9), demonstrating the variability in the number of pixels with detected growing seasons and the timing of the seasons. We also identified low greenness amplitude and high variability in both magnitude and timing of LSP episodes at certain sites, as shown at the demonstration sites in Figure 7.

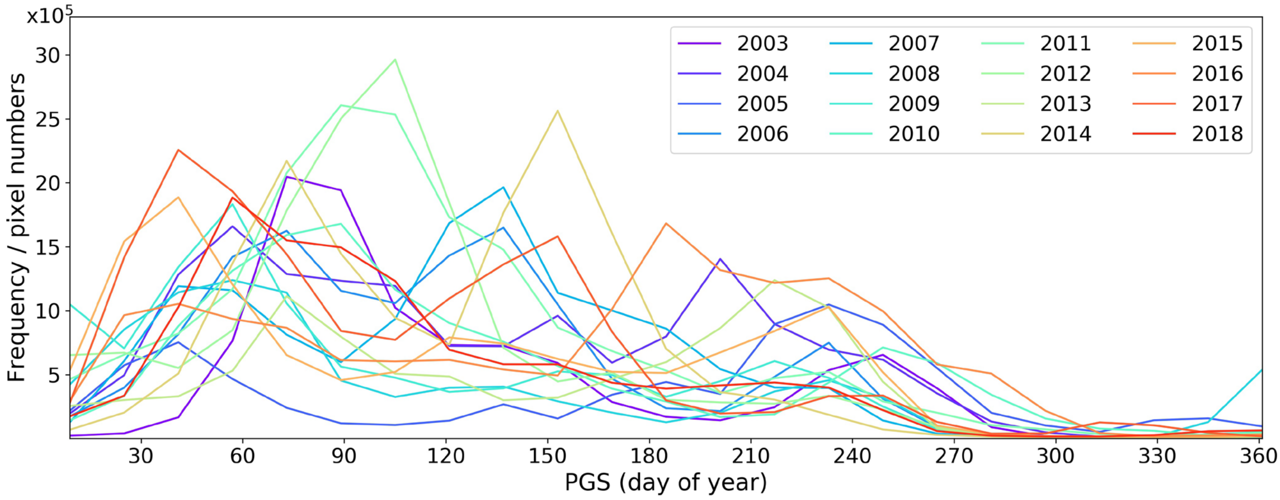

Figure 9. Histogram of the peak of growing season each year from 2003 to 2018 across the study area.

Growing seasons started, peaked, and ended earlier in northern and western edges of our study area than in southern and eastern edges (Figure 10a-c). These phenological timing gradients matched spatial variability in rainfall seasonality (CSIRO and Bureau of Meteorology, 2018). In northern, south-eastern and south-western edges of the semi-arid zone, growing seasons occurred in most years over the 16-year period, whereas patches within the interior areas and along the eastern and central edges had as few as 4–8 years out of 16 with a detectable growing season (Figure 10i). Inter-annual variation (standard errors calculated from the multi-year mean) of SGS, PGS and EGS was largest in central and eastern Australia, reaching 240 days in central Australia, and smallest (30–60 days) in northern areas (Figure 10d–f). In general, variability in PGS was larger than that of EGS, which was larger than that of SGS (Figure 10d–f). The shortest lengths of LGS (90–120 days) were found in eastern semi-arid areas and along the west coast, whereas LGS reached up to 240 days in western areas (Figure 10g). Of all the metrics, LGS had the most uniform variability across the continent, with standard errors which were 60–90 days over the majority of the continent and smaller levels of variability in the south-western and south-eastern corners of the arid and semi-arid zone (Figure 10h).

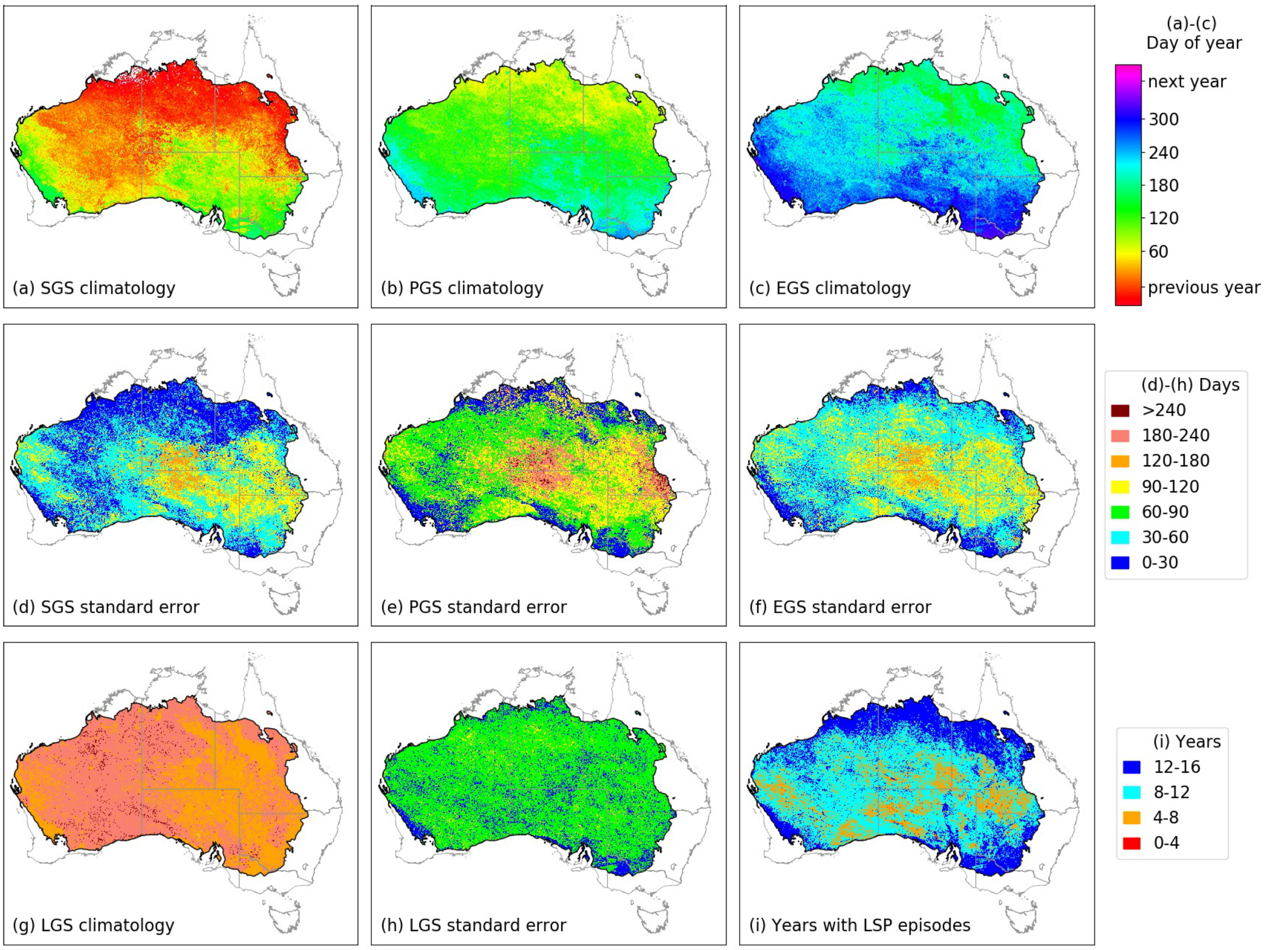

Figure 10. Climatology (average of 16 years) and standard error of SGS, PGS, EGS, and LGS from 2003 to 2018, and years with detected LSP episodes over the 16 years according to our algorithm.

Overall, around 30% of areas were dormant (without showing active growing seasons) in half of the 16 years (Figure 11i). Most pixels showed SGS to occur around the beginning of the year or the end of the previous year (Figure 11a), PGS to occur in the early to middle of the year (Figure 11b), and EGS to occur late in the year (Figure 11c). No narrow period of the growing season timing was observed in these arid and semi-arid ecosystems across 16 years due to high variance (standard error) (Figure 11d–f). As shown in Figure 11d-g, only around 30% of pixels show a standard error of SGS below 30 days and less than 20% of pixels show that of PGS, EGS, and LGS below 30 days.

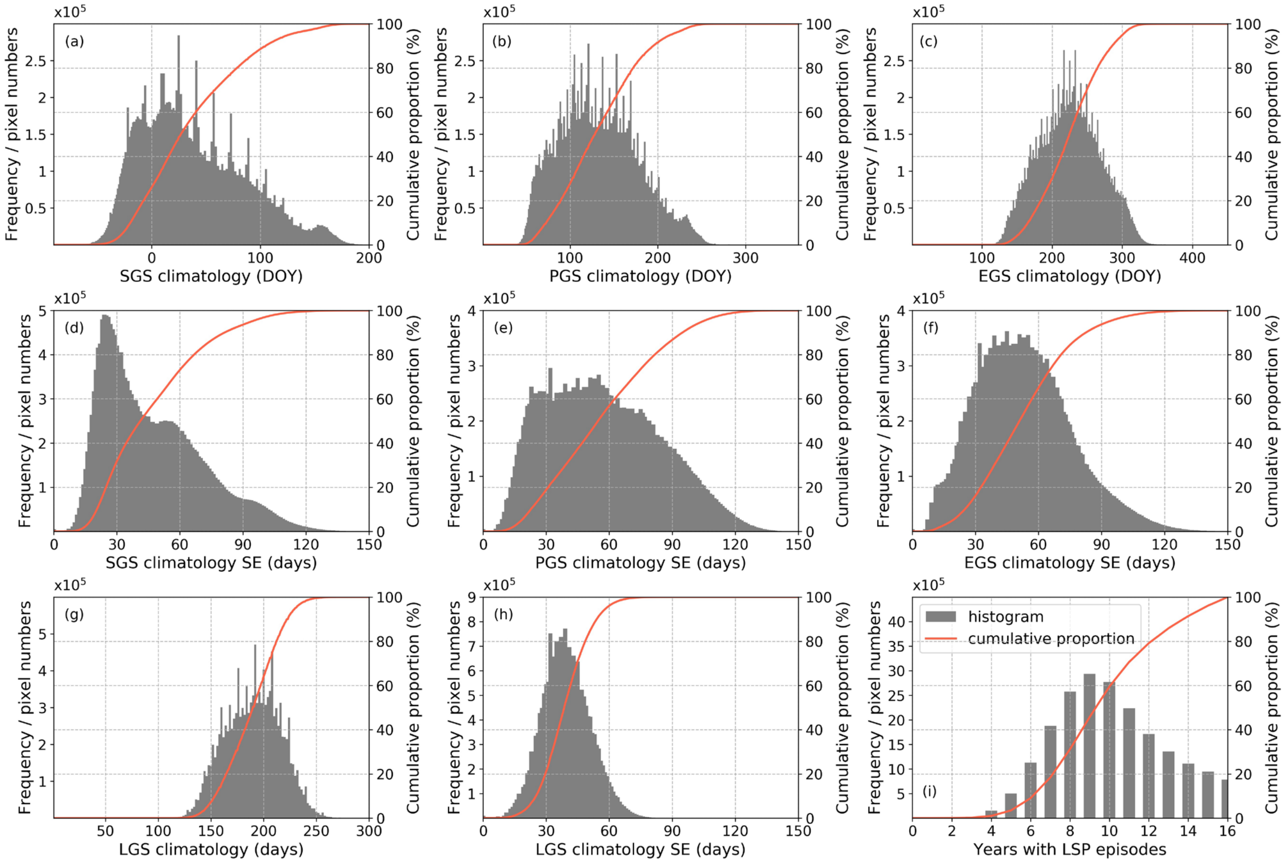

Figure 11. Histogram and cumulative proportion of the climatology and standard error (SE) of SGS, PGS, EGS, and LGS from 2003 to 2018, and years with detected LSP episodes (detected LSP episodes include pixels with both one or two detected growing seasons) over the 16 years according to our algorithm.

Rainfall was found to be associated with the spatial pattern of the LSP in arid and semi-arid Australia through our climate analysis. The correlations between the proportion of pixels with no seasons/one season/two seasons and annual precipitation and annual mean temperature averaged across the entire study area are shown in Figure 12. The proportion of pixels with two seasons each year significantly increased with increasing annual precipitation ($R^2 = 0.64$, $p < 0.01$), i.e. an increase in the proportion of pixels with two growing seasons was associated with higher annual precipitation ($p<0.01$), whereas the proportion of pixels with no seasons each year showed a significant negative correlation to annual precipitation ($R^2 = 0.32$, $p = 0.02$). Temperature also played an important role in regulating LSP, with the proportion of pixels with two seasons significantly decreased as temperature increased ($R^2 = 0.26$, $p = 0.04$) over space.

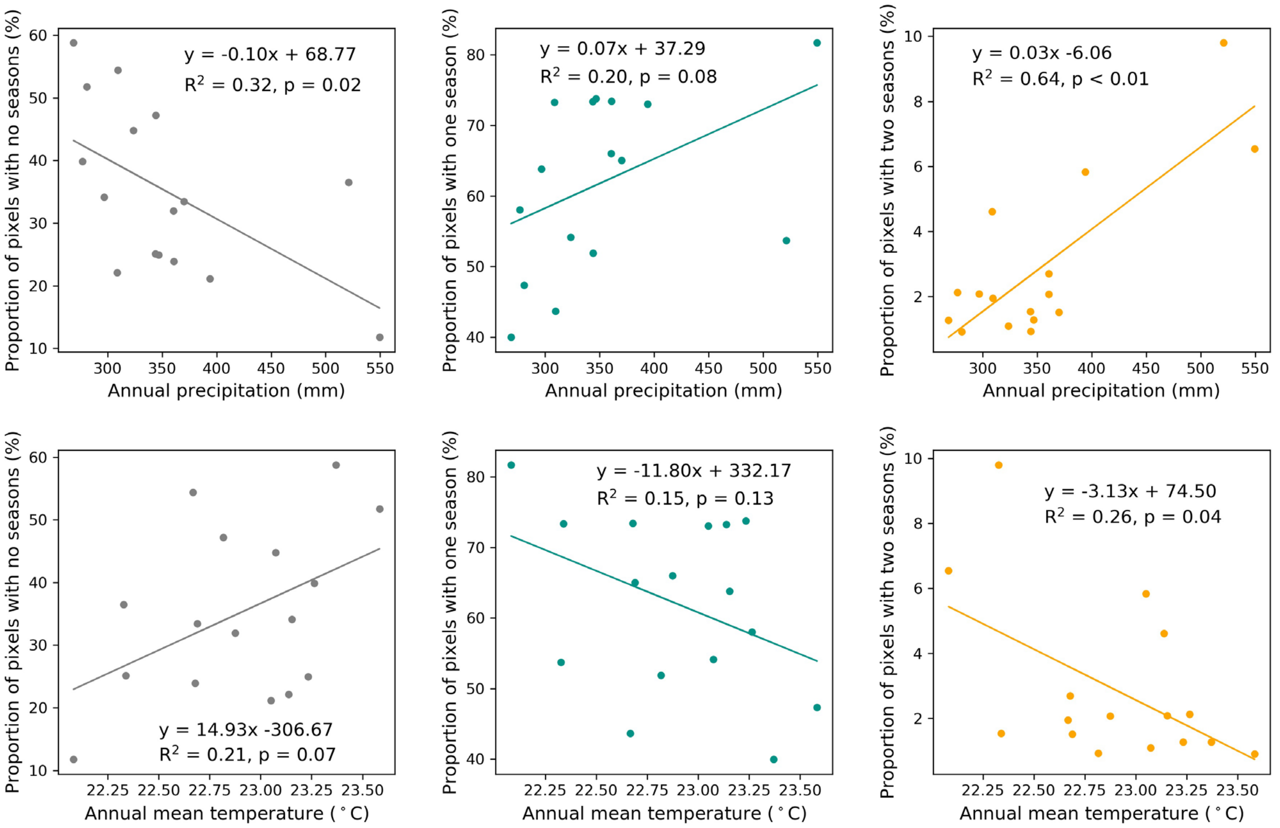

Figure 12. Correlation between proportion of pixels with no seasons/one season/two seasons each year from 2003 to 2018 with annual precipitation and annual mean temperature, respectively. Annual precipitation and annual mean temperature were averaged across the study area. P value was generated using Wald Test.

3.4 Evaluation of the LSP retrieval algorithm

Daily NBAR EVI, 16-day MYD13A1 EVI, and derived SGS and EGS are presented in Figure 13. Among the 80 site-years shown in Figure 13, no vegetation growth was detected in 7 years using both daily NBAR EVI and 16-day EVI retrievals: one year at Sturt Plains (2005), three years at Alice Springs Mulga (2008, 2009, and 2013), two years at Calperum (2014 and 2016), and one year at Yanco (2018). In another 9 years, vegetation growth was only detected by retrievals using either 16-day EVI or daily NBAR EVI (but not both). For example, Alice Springs Mulga in 2018 saw an LSP episode using EVI as input data but no episode was detected when using NBAR EVI. Among the 80 site-years, 65 growing seasons were detected by both our algorithm using both 16-day EVI and daily NBAR EVI. Inter-comparison between SGS, PGS, and EGS retrieved using these two types of input data showed strong correlation with R^2 values above 0.70 and RMSE values of around 30 days (1.9 compositing dates of the 16-day EVI data), as shown in Figure 14.

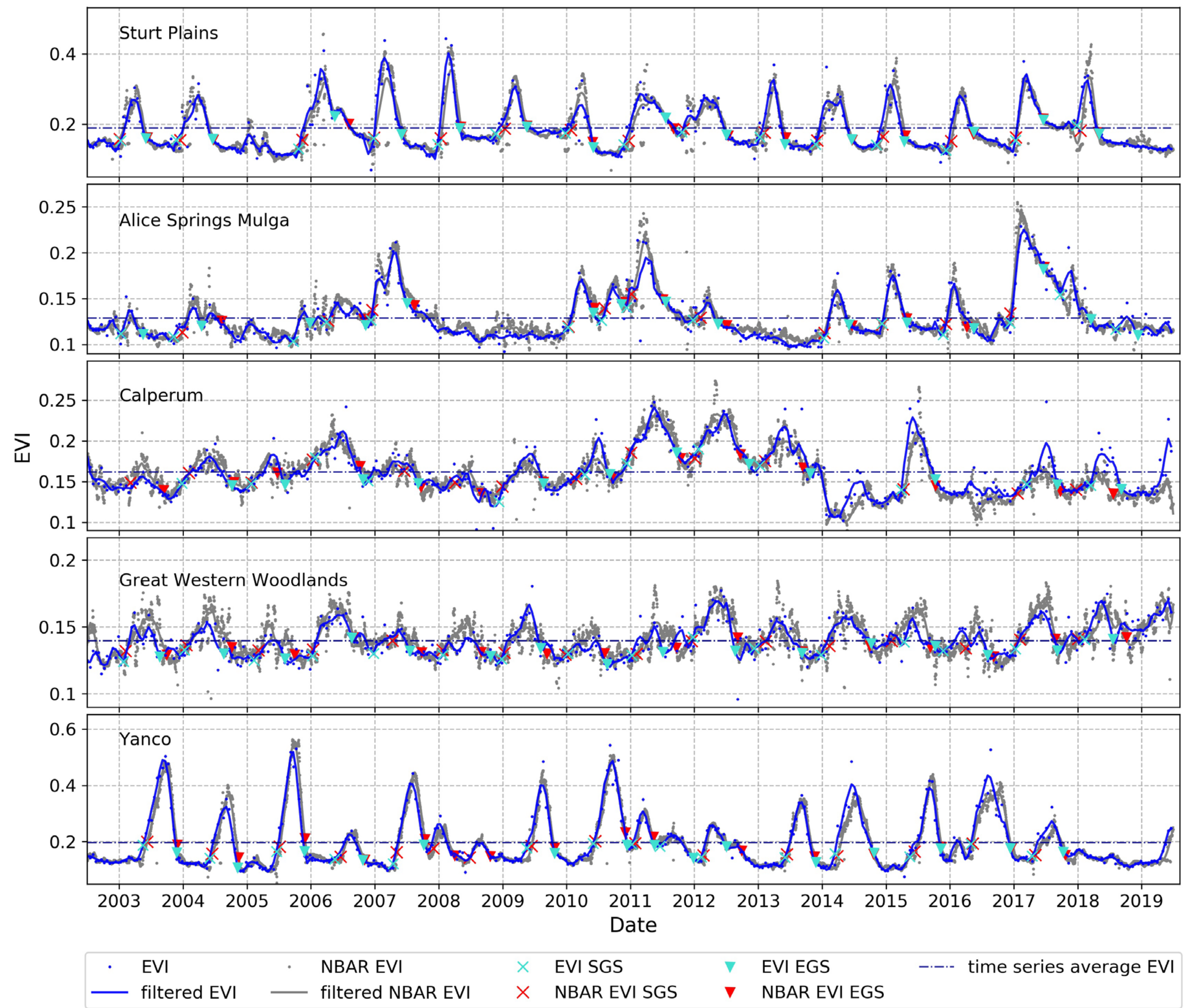

Figure 13. EVI time series and the characterized LSP episodes across 16 years for the five OzFlux sites: Sturt Plains, Alice Springs Mulga, Calperum, Great Western Woodlands, and Yanco. Grey and navy dots represent EVI time series after quality control from daily NBAR EVI and 16-day EVI, respectively. Grey and navy lines represent the EVI time series after gap filling and SG filtering from NBAR EVI and EVI, respectively. Yellow and orange dots represent the identified start and end of growing season points from daily NBAR EVI and 16-day EVI, respectively.

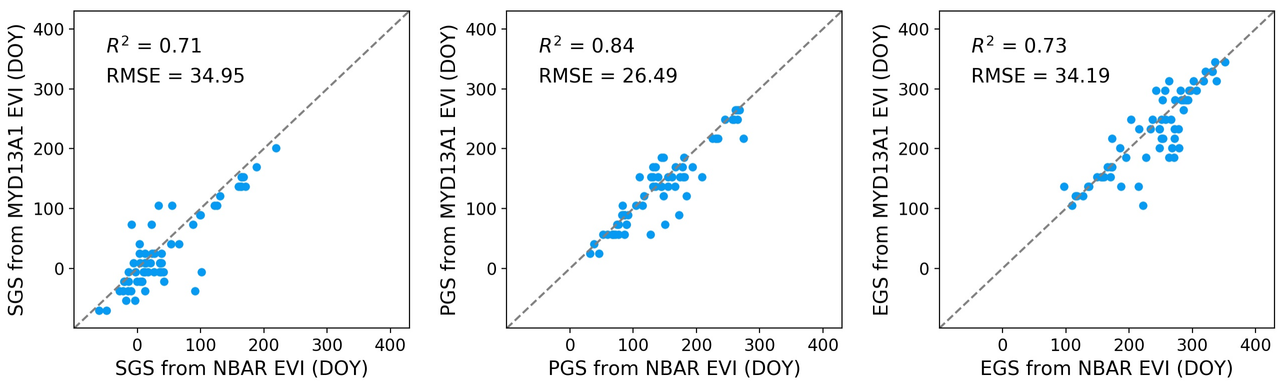

Figure 14. Inter-comparison of phenological metrics from 2003 to 2018 at five OzFlux sites in Table 1, retrieved using 16-day EVI time series against those retrieved from daily NBAR EVI calculated using NBAR reflectance data (n=65). Here day of year (DOY) lower than 0 means days before the beginning of the year, and DOY exceeding 365 are in the next year.

Figure 15 compares retrieved LSP episodes across 16 years from 2003 to 2018 generated using three approaches, i.e. the global product, our original threshold algorithm, and our threshold algorithm with the same restriction of EVI amplitude ≥ 0.1 used by the global product. No growing season was detected with the restriction of EVI amplitude ≥ 0.1 at the three shrubland sites, Alice Springs Mulga, Calperum, and Great Western Woodlands (left columns in Figure 15) with the lowest rainfall, whereas using a lower threshold produced obvious growing seasons in most years at these sites, as confirmed by GPP data (cf. Figure 7, middle columns in Figure 15). However, when applying the restriction of seasonal amplitude EVI ≥ 0.1, similar to the global product, our algorithm failed to retrieve any LSP episodes at these three sites during the 16 years, matching the retrieval rate of the global product (right columns in Figure 15). For the two wetter sites, where phenology is regular with high seasonal amplitude (Sturt Plains and Yanco, Figure 13), the global product provided similar but slightly fewer successful retrievals than those generated by our model. These results demonstrated that in arid and semi-arid ecosystems, vegetation may not show highly dynamic growing seasons with high seasonal amplitudes, thus the restriction that EVI amplitude ≥ 0.1 was a major contributor to generation of missing values in the global product.

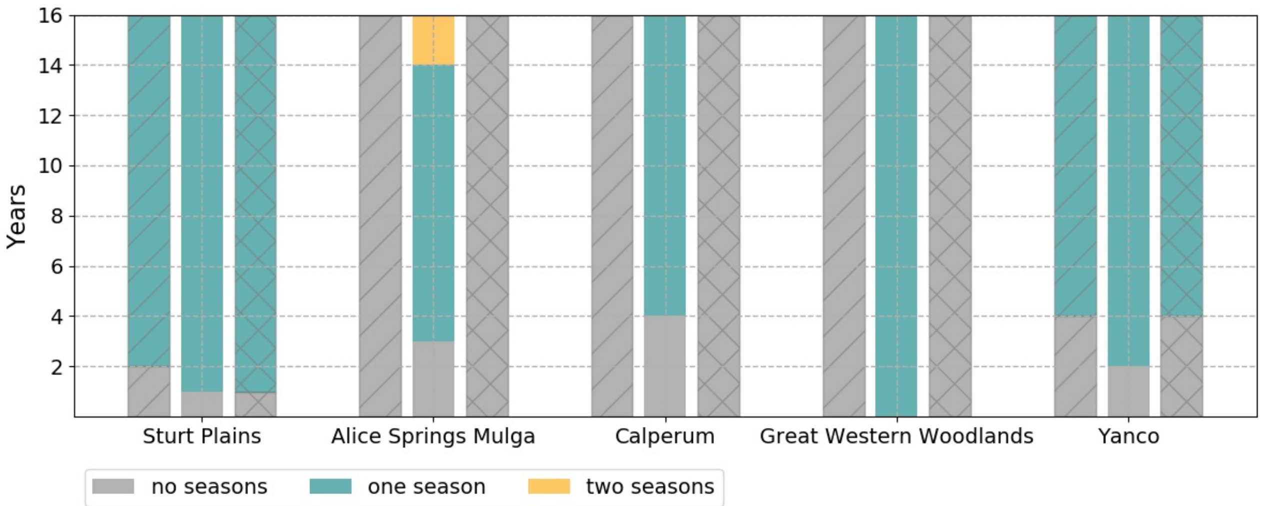

Figure 15. Comparison of the LSP episodes over 16 years from 2003 to 2018 generated from AS-AUS and the global product at the five arid and semi-arid sites. Left column: the global product; middle column: AS-AUS generate using our threshold algorithm in this study; right column: our threshold algorithm with restrictions of seasonal amplitude EVI ≥ 0.1.

4 Discussion

4.1 Algorithm performance

The new amplitude restriction of the threshold algorithm implemented in our study detected phenological information from satellite EVI data across arid and semi-arid Australia. Through inter-comparison with the global product, the LSP metrics for areas where both algorithms succeeded showed high consistency, however, the threshold algorithm used in our study showed much higher rate of retrievals (RoR). In other words, our regionally customized phenometrics extraction algorithm yielded LSP results in larger spatial extent in arid and semi-arid areas in Australia. These LSP retrievals by our model provide us valuable information for understanding the biomes in this vast area, and the connection between vegetation dynamics and climate change. For example, the highest proportion of areas with growing seasons occurred in 2011 (cf. Figure 3b), which was in line with the La Niña in 2010-2011 that caused flooding. The proportion of areas with LSP episodes was at one of its lowest values in 2003, associated with El Niño-induced decadal droughts (Broich et al., 2015). In this study, we found an increase in the proportion of pixels with two growing seasons ($p<0.05$) in arid and semi-arid Australia was associated with higher annual precipitation (averaged across the study area). Some studies have highlighted the significance of sub-annual rainfall on vegetation greenness in drylands (Shen et al., 2015; Ukkola et al., 2021). Future work should include climate analysis using seasonal rainfall in addition to annual rainfall.

Studies have reported that in ecosystems driven by precipitation pulses, like interior Australia, a pulse in net ecosystem productivity follows rainfall events by several days if the rainfall threshold for physiological activity has been met (Cleverly et al., 2016a). Our findings agree with previous studies that phenology can be highly irregular in arid and semi-arid ecosystems (Ma et al., 2013; Beringer et al., 2016; Wang et al., 2019). Our LSP metrics will enable such studies across the arid and semi-arid regions to test these hypotheses at large scales, and therefore, will enhance our understanding of vegetation responses to climate change and assist our prediction of vegetation growth in future climate conditions in these arid and semi-arid ecosystems.

Cross-comparison between the satellite-derived phenological timing metrics and those generated using EC flux tower GPP confirmed the seasons retrieved using satellite greenness data were real seasons. Almost all retrieved seasons showed a 16-year average LGS above 100 days (cf. Figure 1110g), demonstrating that the growing seasons were consistently green for more than 100 days, thus were real, biological active seasons rather than random artefacts. Moreover, most retrieved seasons showed strong association with rainfall, i.e. an increased rainfall around SGS (Figure A1). Note that the second season in a given year could be associated with an earlier rainy season that was shifted from the beginning of the next year to the end of the given year. For example, at the Alice Springs Mulga site, two seasons were detected in 2017 and the second season was associated with rainfall events in late 2017, which was shifted from early 2018 (cf. Figure 3). Cross-comparison with GPP-derived metrics also demonstrated the accuracy of the retrieved seasonal timing metrics, especially at three sites (Sturt Plains, Alice Springs Mulga, and Yanco) located in phenology-driven ecosystems, where changes in the vegetation status drove GPP, and tower-based measurements of photosynthetic activity were best represented by VIs (Restrepo-Coupe et al., 2015). Other studies have also reported strong relationships between vegetation indices and tower GPP in phenology-driven ecosystems such as deciduous forests and grasslands (Rahman et al., 2005; Sjöström et al., 2011). Distinct differences in EVI relationships with tower GPP were found at Calperum (Mediterranean Mallee woodland) and Great Western Woodlands (Temperate Eucalypt woodland) where EVI was poorly correlated with GPP, and where productivity was primarily meteorological-driven (e.g. photosynthetic active radiation, air temperature, and/or precipitation) and photosynthetic activity was not represented by vegetation greenness. In other words, changes in plant greenness do not synchronise with changes in photosynthesis in those ecosystems, e.g. plants with high vegetation greenness values may not have intense photosynthetic activity until rainfall increases. In these meteorological-driven ecosystems, statistical significant relationships were found between the EC tower measures of photosynthetic potential (ecosystem light use efficiency (LUE), photosynthetic capacity (Pc)) and satellite greenness indices, thereby, Pc and LUE may be more suitable than GPP for validation of satellite greenness-derived phenology (Restrepo-Coupe et al., 2016).

The discrepancy in patterns of EVI and GPP could also be attributed to root and wood production. Woody sites, especially if they lack a highly dynamic grass layer, will divert a large proportion of fixed carbon into wood and root production, which is not detected by greenness indices. In contrast, grassland sites (and sparsely wooded sites with a dynamic grassy layer) are likely to display more similar dynamics in their greenness and GPP. Accounting for these differences is critical to a correct interpretation of the relationship between the greenness signature of the vegetation and its physiological properties and thus is essential to using flux tower GPP as an evaluation approach of satellite greenness derived phenology.

In addition, the discrepancy between the metrics generated from EVI and GPP time series could be caused by the spatial-scale inconsistencies between the satellite and EC footprints. Generally, the EC represents the vegetation at a distance of 10 to 30 m from the tower per 1 meter above the surface (e.g., the footprint of Yanco flux tower is approximately 1200 m), whilst the resolution of MODIS/VIIRS EVI data in this study is 500 m (Burba and Anderson, 2010). Moreover, there may be lags between the satellite derived and the EC observed phenology, depending on the main drivers of photosynthetic potential (leaf area index and/or leaf-age). For instance, green-up phases/SGS dominated by leaf-flush will take 2 to 4 weeks to reach the maximum photosynthetic assimilation rate (Chavana-Bryant et al., 2017). Studies have also reported that differences between phenological metrics observed using greenness-based indices and those observed using photosynthesis-based indices could also be attributed to environmental constraints (e.g. radiation limitation) in northern ecosystems (Y. Zhang et al., 2020).

4.2 Algorithm sensitivity

We evaluated the sensitivity of our algorithm to the view angle effects within the input data and restriction of amplitude at five OzFlux sites located across a wide geographical range (133 °E – 146 °E, 17 °S – 35 °S) in arid and semi-arid Australia. Studies have reported the sun and view angle effect on vegetation indices and suggested that an ideal spectral vegetation index should retain maximum sensitivity to plant characteristics while being relatively unaffected by solar angles, topography and viewing direction (Pinter Jr et al., 1987; Ma et al., 2019). In this study, we did not identify major discrepancies between the EVI data with varying view angles from MODIS vegetation index product (MYD13A1) and the NBAR EVI data calculated using MODIS Nadir BRDF-Adjusted Reflectance (NBAR) product (MCD43A4). Only 11% (9 out of 80 site-years observed in total) of the retrievals showed inconsistency in RoR between the outputs using EVI data and those using NBAR EVI data. In those 9 site-years, LSP metrics were generated using either EVI or NBAR EVI, but not by both. Such discrepancies were mostly caused by low seasonal peak values. For instance, at Alice Springs Mulga in 2018, when EVI peak value was slightly above the climatology mean EVI, the growing season was considered by our algorithm as a real season and LSP metrics were retrieved, whilst the NBAR EVI peak value was not higher than the climatology NBAR EVI and thus not considered as a season.

For the 65 site-seasons retrieved using both EVI and NBAR EVI data, the LSP metrics generated using these two types of input data showed strong agreement with each other. Although we are not able to conclusively attribute the difference in LSP detected from these two input data to a specific source, one of the most likely explanations for observed differences in phenological timing is the difference in the temporal resolution of the input data propagated into the LSP metrics, as studies have shown that vegetation phenology detection is sensitive to the temporal resolution of the input data and the accuracy is reduced when the temporal resolution of input satellite data is coarser (Zhang et al., 2009). From preliminary tests at these five sites, our algorithm demonstrated its robustness to view angle-induced sensitivity of input, therefore, view angle differences in input data are not a major reason for the differences in algorithm performance between our study and the global product.

We also tested the amplitude restriction used to generate the global product MCD12Q2 (Collection 6) at the above-mentioned sites. When using the same amplitude restriction (greater than or equal to 0.1) as applied in the global product, our algorithm retrieved fewer LSP episodes at three sites in arid regions. As demonstrated in our study, growing season amplitudes according to EVI values can be lower than 0.1, hence such a restriction on seasonal amplitude could be a major reason for missing values in the global product in arid and semi-arid ecosystems. Previous studies have reported that vegetation cover and heterogeneity are also important factors that could cause challenges to LSP retrieval in arid and semi-arid areas where vegetation greenness is low and using high resolution satellite data can improve LSP retrieval in area with low vegetation cover (Peng et al., 2021). Thus our finding about the amplitude restriction that caused the missing values of the global product in arid and semi-arid Australia indicates that LSP retrieval may also be improved by using higher spatial resolution satellite data such as Landsat and Sentinel-2 (Ke et al., 2015; Melaas et al., 2016; Y. Fu et al., 2019; Bolton et al., 2020) or using harmonized data from both high and low spatial resolution satellites (Walker et al., 2014; X. Zhang et al., 2020), besides using our proposed amplitude restriction in this study.

4.3 Limitations of the algorithm

A known limitation of the threshold algorithm used in our study is that it does not produce LSP metrics when the peak EVI value is lower than the average of multi-year average EVI time series value. This restriction is implemented to prevent our algorithm from retrieving false growing seasons, but this could result in missing values when the amplitude of a certain year is significantly lower than other years, which have high peak EVI values that result in a high multi-year average EVI value. For example, the growing season at Calperum in 2014 was missed by our algorithm, which was the first growing season after part of the area was burnt in January 2014 (Figure 6). On the other hand, this limitation could also result in spurious values, for example at Alice Springs Mulga in 2018, where the multi-year average EVI value is very low and so a minor increase and decrease in EVI value was considered a growing season. As such, this restriction needs further evaluation.

Although simple measures of EC flux tower GPP were closely aligned with satellite greenness at the two grassland sites in semi-arid regions, in arid areas, the dynamics of vegetation may be too complex when focused on diverse vegetation types. As discussed above, careful use of flux tower measures are needed for cross-comparison with satellite phenology retrievals, and the complexity of vegetation dynamics in arid ecosystems call for more sophisticated models using both vegetation greenness and photosynthetic data. For example, at the Calperum site, mature evergreen plants can increase their GPP due to growth apart from green leaves before any change in EVI is observed, as was seen in the post-fire recovery in 2014 (Figure 6). In addition, the temporal resolution of our algorithm is limited by the use of 16-day input MODIS data. The effect of temporal resolution on extracting the LSP metrics is expected to be apparent when comparing the LSP metrics generated from 16-day EVI time series with the metrics retrieved from daily flux tower measurements. A strong validation effort is needed to better understand the ecosystem processes driving phenology and increase the reliability of remote sensing products.

Camera-based phenology observation networks have been established in the US, Japan, and Europe, and are under construction in many other countries for retrieving plant phenology data at landscape or species levels (Nasahara and Nagai, 2015; Peichl et al., 2015; Richardson et al., 2018a). In addition to cross-comparison between remotely sensed metrics of phenological cycles and flux tower time series that measure plant physiological properties (Schwartz et al., 2013), further work has been planned using additional methods and extended observation dataset for validation of remotely sensed metrics of phenological cycles, including time-lapse cameras and ground-based radiation sensors that measure time series canopy spectral/greenness (Richardson et al., 2007, 2018b) as well as high resolution satellite images including Landsat, Sentinel-2, and CubeSat (Cheng et al., 2020; Wang et al., 2020; Dixon et al., 2021; Moon et al., 2021).

5 Conclusion

This paper presents Arid and Semi-arid AUStralia Land Surface Phenology (AS-AUS LSP) retrievals using a regionally customized approach -- a modified threshold algorithm, which significantly improved the rate of successful retrieval (% of pixels with successfully retrieved LSP metrics) over a wide geographical range (112 °E – 147 °E, 15 °S – 37 °S) when compared to the Collection 6 MODIS Global Land Cover Dynamics Product MCD12Q2, whereby the seasonal amplitude restriction (EVI amplitude ≥ 0.1) was a major factor that caused missing values of the global product. The threshold algorithm characterized phenological metrics annually from 2003 to 2018 using 16-day EVI time series obtained from MODIS at 500 m resolution. Preliminary tests at five OzFlux showed that our algorithm was robust to input data-induced sensitivity to view angles by delivering consistent LSP retrievals when using NBAR EVI time series as a comparison. Cross-comparison with seasons extracted using EC tower GPP data demonstrated the ability of this algorithm to detect phenological metrics with high accuracy in the face of the irregular seasonal patterns of vegetation growth associated with arid and semi-arid regions. The LSP metrics show that land surface phenology in the arid and semi-arid interior of Australia is highly variable inter-annually and can be non-annual, and that there are plants greening up/browning down throughout the year across Australia.

Our study improved the spatial extent of LSP retrieval in arid and semi-arid ecosystems and thus meets the urgent need to understand how the arid and semi-arid ecosystems adapt to environmental variability.

The AS-AUS LSP metrics provide important information for land management and climate change studies, and assist monitoring of ecosystem carbon exchange and vegetation composition in future climate conditions, and management of bushfires. Our findings should also help advance phenological research in other regions with extensive drylands, such as Africa, the Middle East, and Central Asia, thus further contributing to our understanding of dryland phenological dynamics globally.

Acknowledgement

This study was supported by the Terrestrial Ecosystems Research Network (TERN) Australian landscape phenology and vegetation dynamics for climate resilience, ecosystem services, and forecasting project (CSIRO - C013420) and the Australian Research Council's Discovery Projects funding schemes (DP170101630, DP210100347), and flux data were supported by the Australian government through TERN Ecosystem Processes. Qiaoyun Xie acknowledges support from University of Technology Sydney Chancellor's Postdoctoral Research Fellowship. Yanling Ding acknowledges the support from the Fundamental Research Funds for the Central Universities (Project No.2412020FZ004). Xuanlong Ma acknowledges the support from the Fundamental Research Funds for the Central Universities (lzujbky-2021-ct11). Cong Wang acknowledges the support from the Fundamental Research Funds for the Central Universities (Project No. 30106210182, CCNU21XJ028). We thank the anonymous reviewers for their valuable comments and suggestions.

Reference

Aires, L.M.I., Pio, C.A., Pereira, J.S., 2008. Carbon dioxide exchange above a Mediterranean C3/C4 grassland during two climatologically contrasting years. Glob Chang Biol 14, 539–555.

Australian Bureau of Meteorology, 2016. Climate classification maps [WWW Document], Bureau of Meteorology, Australian Government, Canberra, ACT. https://doi.org/http://www.bom.gov.au/jsp/ncc/climate_averages/climate-classifications/index.jsp?maptype=kpngrp#maps

Australian Bureau of Meteorology, 2014. Climate of Australia. Bureau of Meteorology, Australian Government, Canberra, ACT.

Baldocchi, D., Falge, E., Gu, L., Olson, R., Hollinger, D., Running, S., Anthoni, P., Bernhofer, C., et al., 2001. FLUXNET: A new tool to study the temporal and spatial variability of ecosystem-scale carbon dioxide, water vapor, and energy flux densities. Bulletin of the American Meteorological Society 82, 2415–2434.

Beringer, 2013a. Sturt Plains OzFlux tower site OzFlux: Australian and New Zealand Flux Research and Monitoring hdl: 102.100.100/14230.

Beringer, 2013b. Yanco JAXA OzFlux tower site OzFlux: Australian and New Zealand Flux Research and Monitoring hdl: 102.100.100/14235.

Beringer, J., Hacker, J., Hutley, L.B., Leuning, R., Arndt, S.K., Amiri, R., Bannehr, L., Cernusak, L.A., et al., 2011. Special - Savanna patterns of energy and carbon integrated across the landscape. Bulletin of the American Meteorological Society 92, 1467–1485. https://doi.org/10.1175/2011BAMS2948.1

Beringer, J., Hutley, L.B., Abramson, D., Arndt, S.K., Briggs, P., Bristow, M., Canadell, J.G., Cernusak, L.A., et al., 2015. Fire in Australian savannas: From leaf to landscape. Global Change Biology 21, 62–81. https://doi.org/10.1111/gcb.12686

Beringer, J., Hutley, L.B., McHugh, I., Arndt, S.K., Campbell, D., Cleugh, H.A., Cleverly, J., De Dios, V.R., et al., 2016. An introduction to the Australian and New Zealand flux tower network - OzFlux. Biogeosciences 13, 5895–5916. https://doi.org/10.5194/bg-13-5895-2016

Beringer, J., McHugh, I., Hutley, L.B., Isaac, P., Kljun, N., 2017. Dynamic INtegrated Gap-filling and partitioning for OzFlux (DINGO). Biogeosciences 14, 1457–1460.

Bolton, D.K., Gray, J.M., Melaas, E.K., Moon, M., Eklundh, L., Friedl, M.A., 2020. Continental-scale land surface phenology from harmonized Landsat 8 and Sentinel-2 imagery. Remote Sensing of Environment 240, 111685. https://doi.org/10.1016/J.RSE.2020.111685

Broich, M., Huete, A., Paget, M., Ma, X., Tulbure, M., Coupe, N.R., Evans, B., Beringer, J., et al., 2015. A spatially explicit land surface phenology data product for science, monitoring and natural resources management applications. Environmental Modelling & Software 64, 191–204. https://doi.org/10.1016/j.envsoft.2014.11.017

Buitenwerf, R., Rose, L., Higgins, S.I., 2015. Three decades of multi-dimensional change in global leaf phenology. Nature Climate Change 5, 364–368. https://doi.org/10.1038/nclimate2533

Burba, G., Anderson, D., 2010. A brief practical guide to eddy covariance flux measurements: principles and workflow examples for scientific and industrial applications. Li-Cor Biosciences.

Cao, R., Chen, J., Shen, M., Tang, Y., 2015. An improved logistic method for detecting spring vegetation phenology in grasslands from MODIS EVI time-series data. Agricultural and Forest Meteorology 200, 9–20. https://doi.org/10.1016/j.agrformet.2014.09.009

Chavana-Bryant, C., Malhi, Y., Wu, J., Asner, G.P., Anastasiou, A., Enquist, B.J., Caravasi, E.G.C., Doughty, C.E., et al., 2017. Leaf aging of Amazonian canopy trees as revealed by spectral and physiochemical measurements. New Phytologist 214, 1049–1063.

Cheng, Y., Vrieling, A., Fava, F., Meroni, M., Marshall, M., Gachoki, S., 2020. Phenology of short vegetation cycles in a Kenyan rangeland from PlanetScope and Sentinel-2. Remote Sensing of Environment 248, 112004. https://doi.org/10.1016/j.rse.2020.112004

Cleverly, J., 2011. Alice Springs Mulga OzFlux site OzFlux: Australian and New Zealand Flux Research and Monitoring hdl: 102.100.100/14217.

Cleverly, J., Eamus, D., Restrepo Coupe, N., Chen, C., Maes, W., Li, L., Faux, R., Santini, N.S., et al., 2016a. Soil moisture controls on phenology and productivity in a semi-arid critical zone. Science of the Total Environment 568, 1227–1237. https://doi.org/10.1016/j.scitotenv.2016.05.142

Cleverly, J., Eamus, D., Van Gorsel, E., Chen, C., Rumman, R., Luo, Q., Coupe, N.R., Li, L., et al., 2016b. Productivity and evapotranspiration of two contrasting semiarid ecosystems following the 2011 global carbon land sink anomaly. Agricultural and Forest Meteorology 220, 151–159.

Cleverly, J., Isaac, P., 2018. Bilby TS Time series quality control and analyst, version 1.0. GitHub repository. https://doi.org/10.5281/zenodo.1284606

CSIRO, Bureau of Meteorology, A.G., 2018. State of the Climate 2018.

Davis, J., Pavlova, A., Thompson, R., Sunnucks, P., 2013. Evolutionary refugia and ecological refuges: key concepts for conserving Australian arid zone freshwater biodiversity under climate change. Global Change Biology 19, 1970–1984.

Delbart, N., Beaubien, E., Kergoat, L., Le Toan, T., 2015. Comparing land surface phenology with leafing and flowering observations from the PlantWatch citizen network. Remote Sensing of Environment 160, 273–280.

Didan, K., Munoz, A.B., Solano, R., Huete, A., 2015. MODIS vegetation index user's guide (MOD13 series). University of Arizona: Vegetation Index and Phenology Lab.

Dixon, D.J., Callow, J.N., Duncan, J.M.A., Setterfield, S.A., Pauli, N., Cheng, Y., Vrieling, A., Fava, F., et al., 2021. Satellite prediction of forest flowering phenology. Remote Sensing of Environment 255, 112197. https://doi.org/10.1016/j.rse.2020.112197

Dougherty, R.L., Edelman, A.S., Hyman, J.M., 1989. Nonnegativity-, monotonicity-, or convexity-preserving cubic and quintic Hermite interpolation. Mathematics of Computation 52, 471–494.

Eamus, D., Huete, A., Cleverly, J., Nolan, R.H., Ma, X., Tarin, T., Santini, N.S., 2016. Mulga, a major tropical dry open forest of Australia: recent insights to carbon and water fluxes. Environmental Research Letters 11. https://doi.org/10.1088/1748-9326/11/12/125011

Ehleringer, J.R., Cerling, T.E., Helliker, B.R., Buisson, E., Le Stradic, S., Silveira, F.A.O.O., Durigan, G., Overbeck, G.E., et al., 2019. No trends in spring and autumn phenology during the global warming hiatus. Scientific Reports 10, 1–10. https://doi.org/10.1038/s41467-019-10235-8

Friedl, M., Gray, J., Sulla-Menashe, D., 2019. MCD12Q2 MODIS/Terra+ Aqua Land Cover Dynamics Yearly L3 Global 500m SIN Grid V006 [Data set]. NASA EOSDIS Land Processes DAAC.

Fu, Y., Li, J., Weng, Q., Zheng, Q., Li, L., Dai, S., Guo, B., 2019. Characterizing the spatial pattern of annual urban growth by using time series Landsat imagery. Science of The Total Environment 666, 274–284.

Fu, Z., Stoy, P.C., Poulter, B., Gerken, T., Zhang, Z., Wakbulcho, G., Niu, S., 2019. Maximum carbon uptake rate dominates the interannual variability of global net ecosystem exchange. Global Change Biology 25, 3381–3394. https://doi.org/10.1111/gcb.14731

Ganguly, S., Friedl, M.A., Tan, B., Zhang, X., Verma, M., 2010. Land surface phenology from MODIS: Characterization of the Collection 5 global land cover dynamics product. Remote Sensing of Environment 114, 1805–1816.

Gitelson, A.A., Keydan, G.P., Merzlyak, M.N., 2006. Three-band model for noninvasive estimation of chlorophyll, carotenoids, and anthocyanin contents in higher plant leaves. Geophysical Research Letters 33.

Gray, J., Sulla-Menashe, D., Friedl, M.A., 2019. User Guide to Collection 6 MODIS Land Cover Dynamics (MCD12Q2)

Product. User Guide 6, 1–8.
Heberger, M., 2012. Australia's millennium drought: Impacts and responses. The World's Water. Springer, 97–125.
Henebry, G.M., de Beurs, K.M., 2013. Remote sensing of land surface phenology: A prospectus. Phenology: An Integrative Environmental Science. Springer, 385–411.
Huete, A., Didan, K., Miura, T., Rodriguez, E.P., Gao, X., Ferreira, L.G., 2002. Overview of the radiometric and biophysical performance of the MODIS vegetation indices. Remote Sensing of Environment 83, 195–213.
Huete, A., Justice, C., Van Leeuwen, W., 1999. MODIS vegetation index (MOD 13) algorithm theoretical basis document (ATBD) Version 3.0. EOS Project Office 2.
Hughes, L., 2011. Climate change and Australia: Key vulnerable regions. Regional Environmental Change 11, 189–195. https://doi.org/10.1007/s10113-010-0158-9
Isaac, P., Cleverly, J., McHugh, I., Van Gorsel, E., Ewenz, C., Beringer, J., 2017. OzFlux data: Network integration from collection to curation. Biogeosciences 14, 2903–2928. https://doi.org/10.5194/bg-14-2903-2017
James, J.J., Sheley, R.L., Erickson, T., Rollins, K.S., Taylor, M.H., Dixon, K.W., 2013. A systems approach to restoring degraded drylands. Journal of Applied Ecology 50, 730–739.
Ke, Y., Im, J., Lee, J., Gong, H., Ryu, Y., 2015. Characteristics of Landsat 8 OLI-derived NDVI by comparison with multiple satellite sensors and in-situ observations. Remote Sensing of Environment 164, 298–313.
Keenan, T.F., Richardson, A.D., 2015. The timing of autumn senescence is affected by the timing of spring phenology: Implications for predictive models. Global Change Biology 21, 2634–2641. https://doi.org/10.1111/gcb.12890
Kennedy, R.E., Andréfouët, S., Cohen, W.B., Gómez, C., Griffiths, P., Hais, M., Healey, S.P., Helmer, E.H., et al., 2014. Bringing an ecological view of change to Landsat-based remote sensing. Frontiers in Ecology and the Environment 12, 339–346.
Liang, L., Schwartz, M.D., 2009. Landscape phenology: an integrative approach to seasonal vegetation dynamics. Landscape Ecology 24, 465–472.
Linderholm, H.W., 2006. Growing season changes in the last century. Agricultural and Forest Meteorology 137, 1–14.
Liu, Y., Hill, M.J., Zhang, X., Wang, Z., Richardson, A.D., Hufkens, K., Filippa, G., Baldocchi, D.D., et al., 2017. Using data from Landsat, MODIS, VIIRS and PhenoCams to monitor the phenology of California oak/grass savanna and open grassland across spatial scales. Agricultural and Forest Meteorology 237–238, 311–325. https://doi.org/10.1016/j.agrformet.2017.02.026
Lymburner, L., Tan, P., Mueller, N., Thackway, R., Lewis, A., Thankappan, M., Randall, L., Islam, A., Senarath, U., 2011. The National Dynamic Land Cover Dataset. Geoscience Australia, Symonston, Australia 10.
Ma, X., Huete, A., Moran, S., Ponce-Campos, G., Eamus, D., 2015. Abrupt shifts in phenology and vegetation productivity under climate extremes. Journal of Geophysical Research: Biogeosciences 120, 2036–2052.
Ma, X., Huete, A., Tran, N.N., 2019. Interaction of seasonal sun-angle and savanna phenology observed and modelled using MODIS. Remote Sensing 11, 1–19. https://doi.org/10.3390/rs11121398
Ma, X., Huete, A., Yu, Q., Coupe, N.R., Davies, K., Broich, M., Ratana, P., Beringer, J., et al., 2013. Spatial patterns and temporal dynamics in savanna vegetation phenology across the North Australian Tropical Transect. Remote Sensing of Environment 139, 97–115. https://doi.org/10.1016/j.rse.2013.07.030
MacFarlane, C., 2013. Great Western Woodlands OzFlux: Australian and New Zealand Flux Research and Monitoring hdl: 102.100.100/14226.
Melaas, E.K., Friedl, M.A., Zhu, Z., 2013. Detecting interannual variation in deciduous broadleaf forest phenology using Landsat TM/ETM+ data. Remote Sensing of Environment 132, 176–185. https://doi.org/10.1016/j.rse.2013.01.011
Melaas, E.K., Sulla-Menashe, D., Gray, J.M., Black, T.A., Morin, T.H., Richardson, A.D., Friedl, M.A., 2016. Multisite analysis of land surface phenology in North American temperate and boreal deciduous forests from Landsat. Remote Sensing of Environment 186, 452–464. https://doi.org/10.1016/j.rse.2016.09.014
Moon, M., Richardson, A.D., Friedl, M.A., 2021. Multiscale assessment of land surface phenology from harmonized Landsat 8 and Sentinel-2, PlanetScope, and PhenoCam imagery. Remote Sensing of Environment 266, 112716. https://doi.org/10.1016/j.rse.2021.112716
Moon, M., Zhang, X., Henebry, G.M., Liu, L., Gray, J.M., Melaas, E.K., Friedl, M.A., 2019. Long-term continuity in land surface phenology measurements: A comparative assessment of the MODIS land cover dynamics and VIIRS land surface phenology products. Remote Sensing of Environment 226, 74–92. https://doi.org/10.1016/j.rse.2019.03.034
Moore, C.E., Brown, T., Keenan, T.F., Duursma, R.A., Van Dijk, A.I.J.M., Beringer, J., Culvenor, D., Evans, B., et al., 2016. Reviews and syntheses: Australian vegetation phenology: New insights from satellite remote sensing and digital repeat photography. Biogeosciences 13, 5085–5102. https://doi.org/10.5194/bg-13-5085-2016
Myneni, R.B., Keeling, C.D., Tucker, C.J., Asrar, G., Nemani, R.R., 1997. Increased plant growth in the northern high latitudes from 1981 to 1991. Nature 386, 698.
Nasahara, K.N., Nagai, S., 2015. Review: Development of an in situ observation network for terrestrial ecological remote sensing: the Phenological Eyes Network (PEN). Ecological Research 30, 211–223. https://doi.org/10.1007/s11284-014-1239-x
Peichl, M., Sonnentag, O., Nilsson, M.B., 2015. Bringing color into the picture: using digital repeat photography to

investigate phenology controls of the carbon dioxide exchange in a boreal mire. Ecosystems 18, 115–131.
Peng, D., Wang, Y., Xian, G., Huete, A.R., Huang, W., Shen, M., Wang, F., Yu, L., et al., 2021. Investigation of land surface phenology detections in shrublands using multiple scale satellite data. Remote Sensing of Environment 252. https://doi.org/10.1016/j.rse.2020.112133
Peng, D., Zhang, X., Wu, C., Huang, W., Gonsamo, A., Huete, A.R., Didan, K., Tan, B., et al., 2017. Intercomparison and evaluation of spring phenology products using National Phenology Network and AmeriFlux observations in the contiguous United States. Agricultural and Forest Meteorology 242, 33–46. https://doi.org/10.1016/j.agrformet.2017.04.009
Pinter Jr, P.J., Zipoli, G., Maracchi, G., Reginato, R.J., 1987. Influence of topography and sensor view angles on NIR/red ratio and greenness vegetation indices of wheat. International Journal of Remote Sensing 8, 953–957.
Poulter, B., Frank, D., Ciais, P., Myneni, R.B., Andela, N., Bi, J., Broquet, G., Canadell, J.G., et al., 2014. Contribution of semi-arid ecosystems to interannual variability of the global carbon cycle. Nature 509, 600–603. https://doi.org/10.1038/nature13376
Puma, M.J., Koster, R.D., Cook, B.I., 2013. Phenological versus meteorological controls on land-atmosphere water and carbon fluxes. Journal of Geophysical Research: Biogeosciences 118, 14–29.
Rahman, A.F., Sims, D.A., Cordova, V.D., El-Masri, B.Z., 2005. Potential of MODIS EVI and surface temperature for directly estimating per-pixel ecosystem C fluxes. Geophysical Research Letters 32.
Restrepo-Coupe, N., Huete, A., Davies, K., Cleverly, J., Beringer, J., 2015. MODIS vegetation products as proxies of photosynthetic potential: a look across meteorological and biologic driven ecosystem productivity. Biogeosciences Discussions 12, 19213–19267. https://doi.org/10.5194/bgd-12-19213-2015
Restrepo-Coupe, N., Huete, A., Davies, K., Cleverly, J., Beringer, J., Eamus, D., Van Gorsel, E., Hutley, L.B., Meyer, W.S., 2016. MODIS vegetation products as proxies of photosynthetic potential along a gradient of meteorologically and biologically driven ecosystem productivity. Biogeosciences 13, 5587–5608. https://doi.org/10.5194/bg-13-5587-2016
Richardson, A.D., Hufkens, K., Milliman, T., Aubrecht, D.M., Chen, M., Gray, J.M., Johnston, M.R., Keenan, T.F., et al., 2018a. Tracking vegetation phenology across diverse North American biomes using PhenoCam imagery. Scientific Data 5, 1–24. https://doi.org/10.1038/sdata.2018.28
Richardson, A.D., Hufkens, K., Milliman, T., Frolking, S., 2018b. Intercomparison of phenological transition dates derived from the PhenoCam Dataset V1.0 and MODIS satellite remote sensing. Scientific Reports 8, 5679. https://doi.org/10.1038/s41598-018-23804-6
Richardson, A.D., Jenkins, J.P., Braswell, B.H., Hollinger, D.Y., Ollinger, S. V, Smith, M.-L., 2007. Use of digital webcam images to track spring green-up in a deciduous broadleaf forest. Oecologia 152, 323–334.
Richardson, A.D., Keenan, T.F., Migliavacca, M., Ryu, Y., Sonnentag, O., Toomey, M., 2013. Climate change, phenology, and phenological control of vegetation feedbacks to the climate system. Agricultural and Forest Meteorology 169, 156–173. https://doi.org/10.1016/j.agrformet.2012.09.012
Rogers, C.D.W., Beringer, J., 2017. Describing rainfall in northern Australia using multiple climate indices. Biogeosciences 14, 597–615. https://doi.org/10.5194/bg-14-597-2017
Rouse Jr, J.W., Haas, R.H., Schell, J.A., Deering, D.W., 1974. Monitoring vegetation systems in the Great Plains with ERTS. NASA Special Publication 351, 309.
Savitzky, A., Golay, M.J.E., 1964. Smoothing and differentiation of data by simplified least squares procedures. Analytical Chemistry 36, 1627–1639.
Schaaf, C.B., Gao, F., Strahler, A.H., Lucht, W., Li, X., Tsang, T., Strugnell, N.C., Zhang, X., et al., 2002. First operational BRDF, albedo nadir reflectance products from MODIS. Remote Sensing of Environment 83, 135–148.
Schwartz, M.D., Hanes, J.M., Liang, L., 2013. Comparing carbon flux and high-resolution spring phenological measurements in a northern mixed forest. Agricultural and Forest Meteorology 169, 136–147. https://doi.org/10.1016/j.agrformet.2012.10.014
Shen, M., Piao, S., Cong, N., Zhang, G., Jassens, I.A., 2015. Precipitation impacts on vegetation spring phenology on the Tibetan Plateau. Glob Chang Biol 21, 3647–3656. https://doi.org/10.1111/gcb.12961
Sjöström, M., Ardö, J., Arneth, A., Boulain, N., Cappelaere, B., Eklundh, L., De Grandcourt, A., Kutsch, W.L., et al., 2011. Exploring the potential of MODIS EVI for modeling gross primary production across African ecosystems. Remote Sensing of Environment 115, 1081–1089.
Smith, W.K., Dannenberg, M.P., Yan, D., Herrmann, S., Barnes, M.L., Barron-Gafford, G.A., Biederman, J.A., Ferrenberg, S., et al., 2019. Remote sensing of dryland ecosystem structure and function: Progress, challenges, and opportunities. Remote Sensing of Environment 233, 111401. https://doi.org/10.1016/j.rse.2019.111401
Sun, Q., Meyer, W.S., Koerber, G.R., Marschner, P., 2016. A wildfire event influences ecosystem carbon fluxes but not soil respiration in a semi-arid woodland. Agricultural and Forest Meteorology 226–227, 57–66. https://doi.org/10.1016/j.agrformet.2016.05.019
Tarin, T., Nolan, R.H., Eamus, D., Cleverly, J., 2020. Carbon and water fluxes in two adjacent Australian semi-arid ecosystems. Agricultural and Forest Meteorology 281, 107853.
Tech, C., 2013. Calperum Chowilla OzFlux tower site OzFlux: Australian and New Zealand Flux Research and

Monitoring hdl: 102.100.100/14236.
Thompson, J.A., Paull, D.J., 2017. Assessing spatial and temporal patterns in land surface phenology for the Australian Alps (2000–2014). Remote Sensing of Environment 199, 1–13. https://doi.org/10.1016/j.rse.2017.06.032
Ukkola, A.M., De Kauwe, M.G., Roderick, M.L., Burrell, A., Lehmann, P., Pitman, A.J., 2021. Annual precipitation explains variability in dryland vegetation greenness globally but not locally. Global Change Biology.
Vina, A., Liu, W., Zhou, S., Huang, J., Liu, J., 2016. Land surface phenology as an indicator of biodiversity patterns. Ecological Indicators 64, 281–288.
Vivoni, E.R., 2012. Diagnosing seasonal vegetation impacts on evapotranspiration and its partitioning at the catchment scale during SMEX04–NAME. Journal of Hydrometeorology 13, 1631–1638.
Walker, J.J., de Beurs, K.M., Wynne, R.H., 2014. Dryland vegetation phenology across an elevation gradient in Arizona, USA, investigated with fused MODIS and landsat data. Remote Sensing of Environment 144, 85–97. https://doi.org/10.1016/j.rse.2014.01.007
Wang, C., Beringer, J., Hutley, L.B., Cleverly, J., Li, J., Liu, Q., Sun, Y., 2019. Phenology Dynamics of Dryland Ecosystems Along the North Australian Tropical Transect Revealed by Satellite Solar-Induced Chlorophyll Fluorescence. Geophysical Research Letters 46, 5294–5302. https://doi.org/10.1029/2019GL082716
Wang, J., Yang, D., Detto, M., Nelson, B.W., Chen, M., Guan, K., Wu, S., Yan, Z., Wu, J., 2020. Multi-scale integration of satellite remote sensing improves characterization of dry-season green-up in an Amazon tropical evergreen forest. Remote Sensing of Environment 246, 111865. https://doi.org/10.1016/j.rse.2020.111865
Wang, L., Tian, F., Wang, Y., Wu, Z., Schurgers, G., Fensholt, R., 2018. Acceleration of global vegetation greenup from combined effects of climate change and human land management. Global Change Biology 24, 5484–5499. https://doi.org/10.1111/gcb.14369
Wang, S., Zhang, L., Huang, C., Qiao, N., 2017. An NDVI-Based Vegetation Phenology Is Improved to be More Consistent with Photosynthesis Dynamics through Applying a Light Use Efficiency Model over Boreal High-Latitude Forests. Remote Sensing 9. https://doi.org/10.3390/rs9070695
White, M.A., de Beurs, K.M., Didan, K., Inouye, D.W., Richardson, A.D., Jensen, O.P., O'KEEFE, J., Zhang, G., et al., 2009. Intercomparison, interpretation, and assessment of spring phenology in North America estimated from remote sensing for 1982–2006. Global Change Biology 15, 2335–2359.
White, M.A., Thornton, P.E., Running, S.W., 1997. A continental phenology model for monitoring vegetation responses to interannual climatic variability. Global Biogeochemical Cycles 11, 217–234. https://doi.org/10.1029/97gb00330
Winslow, J.C., Hunt Jr, E.R., Piper, S.C., 2003. The influence of seasonal water availability on global C3 versus C4 grassland biomass and its implications for climate change research. Ecological Modelling 163, 153–173.
Wu, C., Hou, X., Peng, D., Gonsamo, A., Xu, S., 2016. Land surface phenology of China's temperate ecosystems over 1999-2013: Spatial-temporal patterns, interaction effects, covariation with climate and implications for productivity. Agricultural and Forest Meteorology 216, 177–187. https://doi.org/10.1016/j.agrformet.2015.10.015
Xu, X., Riley, W.J., Koven, C.D., Jia, G., 2019. Heterogeneous spring phenology shifts affected by climate: supportive evidence from two remotely sensed vegetation indices. Environmental Research Communications 1, 091004. https://doi.org/10.1088/2515-7620/ab3d79
Yang, X., Huang, P., 2021. Restored relationship between ENSO and Indian summer monsoon rainfall around 1999/2000. The Innovation 2, 100102.
Yu, Y., Mao, J., Thornton, P.E., Notaro, M., Wullschleger, S.D., Shi, X., Hoffman, F.M., Wang, Y., 2020. Quantifying the drivers and predictability of seasonal changes in African fire. Nature Communications 11. https://doi.org/10.1038/s41467-020-16692-w
Zhang, X., 2015. Reconstruction of a complete global time series of daily vegetation index trajectory from long-term AVHRR data. Remote Sensing of Environment 156, 457–472. https://doi.org/10.1016/j.rse.2014.10.012
Zhang, X., Friedl, M.A., Schaaf, C.B., 2009. Sensitivity of vegetation phenology detection to the temporal resolution of satellite data. International Journal of Remote Sensing 30, 2061–2074. https://doi.org/10.1080/01431160802549237
Zhang, X., Friedl, M.A., Schaaf, C.B., 2006. Global vegetation phenology from Moderate Resolution Imaging Spectroradiometer (MODIS): Evaluation of global patterns and comparison with in situ measurements. Journal of Geophysical Research: Biogeosciences 111.
Zhang, X., Friedl, M.A., Schaaf, C.B., Strahler, A.H., Hodges, J.C., Gao, F., Reed, B.C., Huete, A., 2003. Monitoring vegetation phenology using MODIS. Remote Sensing of Environment 84, 471–475.
Zhang, X., Jayavelu, S., Liu, L., Friedl, M.A., Henebry, G.M., Liu, Y., Schaaf, C.B., Richardson, A.D., Gray, J., 2018a. Evaluation of land surface phenology from VIIRS data using time series of PhenoCam imagery. Agricultural and Forest Meteorology 256–257, 137–149. https://doi.org/10.1016/j.agrformet.2018.03.003
Zhang, X., Liu, L., Liu, Y., Jayavelu, S., Wang, J., Moon, M., Henebry, G.M., Friedl, M.A., Schaaf, C.B., 2018b. Generation and evaluation of the VIIRS land surface phenology product. Remote Sensing of Environment 216, 212–229.
Zhang, X., Wang, J., Henebry, G.M., Gao, F., 2020. Development and evaluation of a new algorithm for detecting 30 m land surface phenology from VIIRS and HLS time series. ISPRS Journal of Photogrammetry and Remote Sensing

161, 37–51. https://doi.org/10.1016/j.isprsjprs.2020.01.012
Zhang, Y., Commane, R., Zhou, S., Williams, A.P., Gentine, P., 2020. Light limitation regulates the response of autumn terrestrial carbon uptake to warming. Nature Climate Change 10, 739–743.

Appendix

For each season, monthly rainfall from one month before SGS through one month after SGS was averaged and then compared with the average monthly rainfall from 2003 to 2018. For a given season, if the rainfall around SGS (from one month before SGS through one month after SGS) is above 16-year climatology, it shows that the green-up of this season was associated with an increased rainfall, thus this season is confirmed by rainfall to be a real season. As shown in Figure A1 a, c, most pixels with retrieved seasons showed higher than climatology rainfall around SGS. The histograms (Figure A1 b, d) further reveal that for the majority of pixels (more than 80%), the majority of seasons (more than 50%) showed an above climatology rainfall amount around SGS, which was true for both season 1 and season 2.

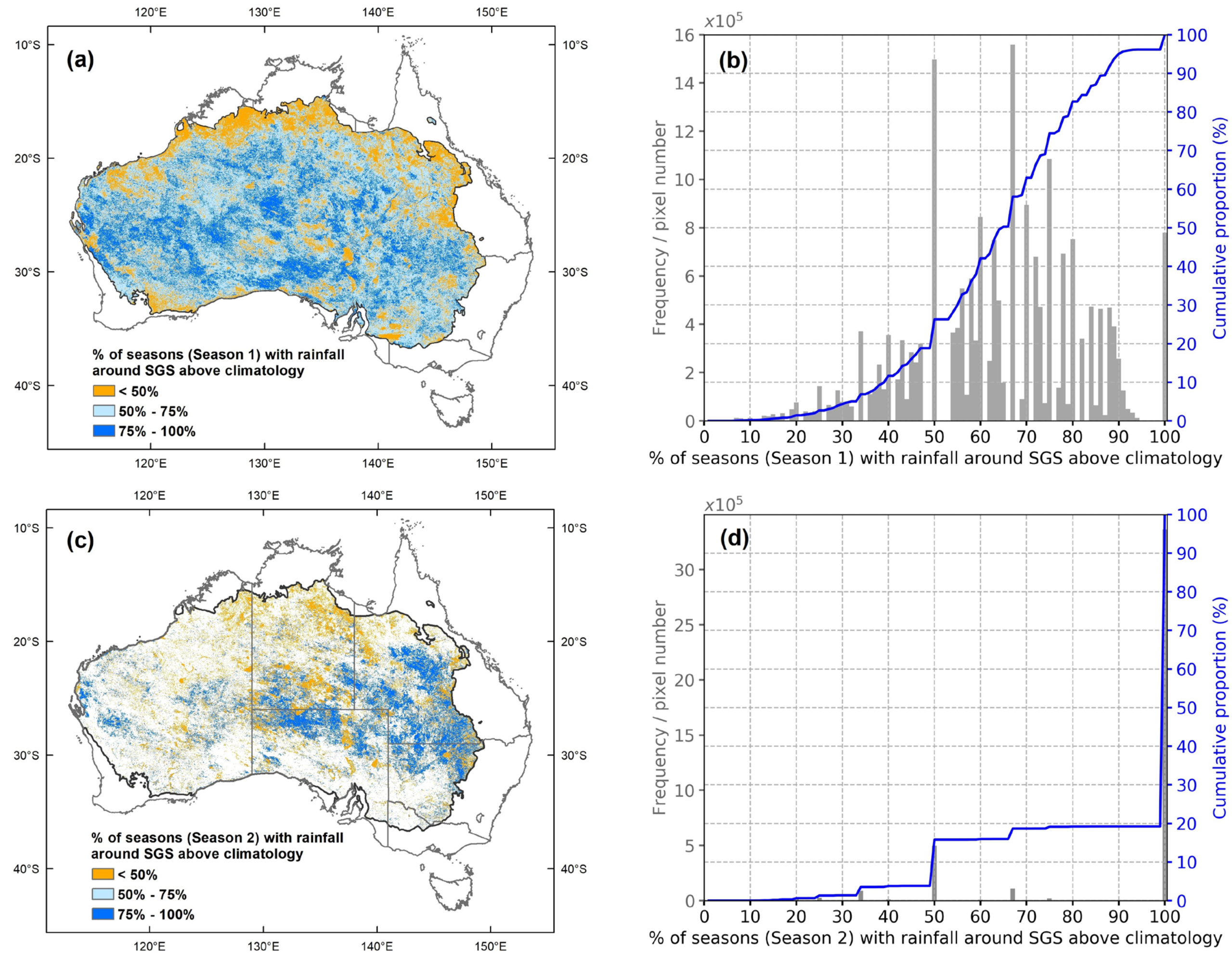

Figure A1. Percent of seasons retrieved by AS-AUS with monthly average rainfall around SGS (from one month before SGS through one month after SGS) above climatology (monthly average rainfall from 2003 to 2018). (a) Map of spatially detailed percent of seasons (Season 1 in each year) retrieved by AS-AUS with monthly average rainfall around SGS above 16-year climatology; (b) Histogram of the map in (a); (c) Map of spatially detailed percent of seasons (Season 2 in each year) retrieved by AS-AUS with monthly average rainfall around SGS above 16-year climatology; (d) Histogram of the map in (c).